Topological hydrodynamics in ferromagnetic superconductors

Chau Dao [1,*] Eric Kleinherbers [1,*] Bjørnulf Brekke [2] and Yaroslav Tserkovnyak [1]
[1]*Department of Physics and Astronomy and Bhaumik Institute for Theoretical Physics, University of California, Los Angeles, California 90095, USA*
[2]*Center for Quantum Spintronics, Department of Physics, NTNU–Norwegian University of Science and Technology, NO-7491 Trondheim, Norway*

(Received 8 August 2025; accepted 20 April 2026; published 15 May 2026)

We explore the physical consequences of enriching the U(1) order parameter of conventional superconductors to a more topologically featureful space. As an illustrative case study, we focus on fully spin-polarized triplet superconductors, which are underlied by the SO(3) **d**-vector order parameter. We find that a bulk-edge correspondence links the circulation of supercurrent to the bulk magnetic skyrmions, giving rise to *topological hydrodynamics* of magnetic skyrmions. To probe the interplay of charge and spin dynamics, we propose a blueprint for a spin-triplet superconducting quantum interference device (SQUID), which functions without a Josephson weak link. The triplet SQUID undergoes *nonsingular* 4π phase slips, in which current relaxation is facilitated by spin dynamics that trace out a magnetic skyrmion texture. Inductively coupling the device to a tank circuit and probing the nonlinear supercurrent response via Oersted field measurements could provide an experimental signature of ferromagnetic spin-triplet superconductivity. Finally, we develop a general Poisson bracket formalism to describe the intertwined spin and charge dynamics such that all topological constraints are preserved, even in the presence of dissipation.

DOI: 10.1103/52jm-l96p

I. INTRODUCTION

One of the most striking features of superconductivity is the indefinite persistence of supercurrent in a closed loop, which is rooted in the topological structure of the underlying U(1) order parameter space [1–4]. Namely, the homotopic classification $\pi_1[\mathrm{U}(1)] = \mathbb{Z}$ informs us that the phase winding along a closed superconducting loop is a topologically protected quantity [4]. Hence, for U(1) superconductors, the only means for the supercurrent (which stems from the spatial phase gradient) to relax is via *singular* phase slip events where the order parameter locally vanishes and the winding number is allowed to change [5].

Singular phase slip processes can occur naturally in thin superconducting nanowires [6,7] or can be facilitated by weak links used, for example, in a superconducting quantum interference device (SQUID) [8]. The resulting phase slips give rise to a finite resistance, accompanied by (potentially unwanted) dissipation of energy [5]. Here, we consider *nonsingular* phase slips, in which the order parameter does not vanish. Such processes can occur in superconductors in which the order parameter space is enriched from U(1) to a more complex space. Unconventional superconductor candidates, such as uranium heavy-fermion compounds [9], bilayer graphene [10–16], and ferromagnet-superconductor heterostructures [9,17–19], may host such enriched order parameters [20–22].

In this work, we focus on ferromagnetic superconductors, which we phenomenologically describe with hydrodynamic variables: superconducting winding $\mathbf{w}(\mathbf{r})$, spin orientation $\mathbf{s}(\mathbf{r})$, and charge density $\rho(\mathbf{r})$. As a case study, we consider a fully spin-polarized triplet superconductor which has an SO(3) order parameter space. This can potentially be realized in bilayer graphene as an *s*-wave, valley-singlet, spin-triplet superconductor [13–15]. As dictated by the structure of the underlying $\mathbf{d}(\mathbf{r})$-vector order parameter [23], the hydrodynamic variables $\{\rho, \mathbf{s}, \mathbf{w}\}$ are intertwined. Continuous (nonsingular) changes in the supercurrent flow can be facilitated by magnetic dynamics and, vice versa, manipulation of the spin texture can give rise to charge dynamics [24–28]. Specifically, we find a bulk-edge correspondence linking the circulation of supercurrent to the bulk magnetic skyrmions [24,25,29]. As a consequence, such spin-triplet superconductors exhibit *topological hydrodynamics* of magnetic skyrmions. These skyrmions can be understood as coreless vortices [30] that initiate a nonsingular phase slip process.

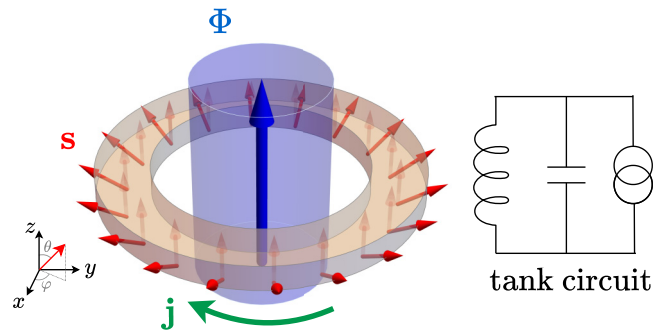

FIG. 1. Superconducting ring (left) with the spin orientation field **s** (red arrows), circulating supercurrent **j** (green arrow), and the magnetic flux (blue arrow), coupled to a tank circuit.

*These authors contributed equally to this work.

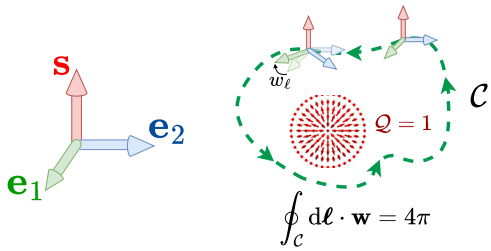

FIG. 2. Sketch of the order parameter **d** via the orthonormal triad $\{\mathbf{e}_1, \mathbf{e}_2, \mathbf{s}\}$ (left) and the bulk-edge correspondence between superconducting winding density **w** and skyrmion charge $\mathcal{Q}$ (right).

To illustrate the consequences of this physics, we propose a minimal setup for a spin-triplet superconducting quantum interference device (SQUID), shown in Fig. 1. Whereas spin-singlet SQUIDs require a Josephson weak link, the spin-triplet SQUID can undergo nonsingular 4π phase slips [5]. Readout can be performed by inductively coupling the spin-triplet SQUID to a tank circuit and probing the supercurrent via Oersted field measurements [31]. This can motivate a signature experiment for spin-polarized triplet superconductivity. Finally, we discuss a more complete dynamical theory based on Poisson brackets that preserves all topological constraints, even in the presence of dissipation.

II. ORDER PARAMETER GEOMETRY

The link between charge and magnetic dynamics is rooted in the structure of the **d**-vector order parameter. In the minimal model of a fully spin-polarized triplet superconductor, the order parameter can be expressed as $\mathbf{d}(\mathbf{r}, t) = d(\mathbf{e}_1 + i\mathbf{e}_2)/\sqrt{2}$, which is a complex vector field of modulus $d \equiv \sqrt{\mathbf{d}\cdot\mathbf{d}^*}$. The orientational degrees of freedom of **d** are captured by

$$\mathbf{s} = \mathbf{e}_1 \times \mathbf{e}_2, \quad \mathbf{w} = (\nabla \mathbf{e}_2)\cdot\mathbf{e}_1. \tag{1}$$

We infer that **s** is the spin-orientation field since it satisfies the spin-commutation algebra (see Sec. IV below). Together with $\mathbf{e}_1$ and $\mathbf{e}_2$, it forms the spatially varying orthonormal triad $\{\mathbf{e}_1, \mathbf{e}_2, \mathbf{s}\}$; see Fig. 2. In addition, $\mathbf{w}(\mathbf{r}, t)$ is the superconducting winding density [32], which tracks rotations of the **d** vector about **s** [33,34]. The orientational degrees of freedom **s** and **w** are the building blocks for our phenomenology. For more details, see Appendix A.

The superconducting winding **w** and the spin-orientation field **s** are related through Stokes' theorem. For a two-dimensional superconducting patch $\mathcal{A}$, we find

$$\mathcal{W} = \int_{\partial\mathcal{A}} \mathrm{d}\boldsymbol{\ell}\cdot\mathbf{w} = \int_{\mathcal{A}} \mathrm{d}A\, \varrho_{\mathrm{sk}}(\mathbf{s}), \tag{2}$$

which has been written using the skyrmion density $\varrho_{\mathrm{sk}}(\mathbf{s}) \equiv \mathbf{s}\cdot(\partial_x\mathbf{s}\times\partial_y\mathbf{s})$. Equation (2) establishes a bulk-edge correspondence between the integrated winding $\mathcal{W}$ along a boundary $\partial\mathcal{A}$ and the skyrmion charge $\mathcal{Q} = \int_{\mathcal{A}} \mathrm{d}A\, \varrho_{\mathrm{sk}}/4\pi$; see Fig. 2. As a skyrmion traverses the boundary $\partial\mathcal{A}$, there is a commensurate change in the superconducting winding. This implies a topological continuity equation for magnetic skyrmions, $\partial_t\varrho_{\mathrm{sk}} = -\nabla\cdot\mathbf{j}_{\mathrm{sk}}$, where $\mathbf{j}_{\mathrm{sk}} = \mathbf{s}\cdot[\partial_t\mathbf{s}\times(\mathbf{z}\times\nabla)\mathbf{s}]$ is the skyrmion flux.

We note that the skyrmion continuity equation is also fulfilled in conventional Heisenberg magnets, which have an S^2 order parameter space. In that context, the continuity equation stems from the bulk homotopy $\pi_2(S^2) = \mathbb{Z}$, rather than from a Stokes' theorem [35]. Therefore, those skyrmions are local objects that may fluctuate in and out of existence if the order parameter is allowed to vanish locally [36]. In contrast, spin-triplet skyrmions do not follow from such an *absolute* homotopy since $\pi_2[\mathrm{SO}(3)] = 0$. Instead, we topologically classify them using the *relative* homotopy $\pi_2[\mathrm{SO}(3), \mathrm{U}(1)] = \mathbb{Z}$, in which the bulk of the real-space domain (homeomorphic to a disk) can explore the full order parameter space SO(3), while the boundary is restricted to U(1) [37–39], i.e., rotations of $\mathbf{e}_1$ and $\mathbf{e}_2$ about a fixed **s**. Therefore, the spin-triplet skyrmions are inherently nonlocal objects determined by the winding on the boundary and cannot be removed by local surgery. This signifies that the skyrmions are coreless vortices [40] that can exhibit long-range interactions [41] and go hand in hand with nonsingular phase slips. A more formal discussion of the relative homotopy and coreless vortices can be found in Appendix B.

By driving a skyrmion flux transverse to an arbitrary one-dimensional loop $\mathcal{C}$ (which may not necessarily be a boundary), the superconducting winding can be tuned to arbitrary values, a mechanism employed in Ref. [25]. This is captured by $\delta\mathcal{W} = \int \mathrm{d}t \int_{\mathcal{C}} \mathrm{d}\ell\, j_{\mathrm{sk}}$, where $j_{\mathrm{sk}} \equiv \mathbf{s}\cdot(\partial_t\mathbf{s}\times\partial_\ell\mathbf{s})$ is the skyrmion flux directed towards the center of the loop, with ℓ being the arc length. Fully moving a skyrmion across the loop completes a 4π nonsingular phase slip. Formally, these nonsingular phase slips are smooth deformations of the **d**-vector field which preserve the topological sector of $\mathcal{C}$, classified according to the edge homotopy $\pi_1[\mathrm{SO}(3)] = \mathbb{Z}_2$ [42]. When the spin texture is uniform along the loop, we recover integer-valued winding of the superconducting phase, such that $\mathcal{W}/2\pi \in \mathbb{Z}$. The two aforementioned topological sectors correspond to the even and odd multiples of 2π winding [43].

III. SPIN-TRIPLET SQUID

The nonsingular phase slips rooted in the bulk-edge correspondence of Eq. (2) can be leveraged to devise the spin-triplet SQUID, which functions without a Josephson weak link. For this, we consider a one-dimensional superconducting ring of length L threaded by external axial magnetic flux localized within the ring (shown in Fig. 1). For the simplest model, the free energy $\mathcal{F}$ is constructed in terms of the soft modes, spin orientation **s**, and winding density $w = \mathbf{e}_1\cdot\partial_\ell\mathbf{e}_2$, as

$$\mathcal{F}[\mathbf{s}, w] = \int \mathrm{d}\ell \left[\frac{A}{2}(\partial_\ell\mathbf{s})^2 + \frac{1}{2\chi_w}\left(w - \frac{qA_\ell}{\hbar c}\right)^2\right], \tag{3}$$

where, for the moment, we suppress the dependence on charge density (per unit length) ρ. The first term is the spin exchange energy with spin stiffness A. The second term is the superconducting winding energy, with χ_w being the winding compressibility and $q = -2e$ being the Cooper pair charge.

Minimal coupling of the superconducting winding to the magnetic vector potential A_ℓ gives rise to the gauge-independent supercurrent, $j = -c\delta_{A_\ell}\mathcal{F} = (q/\hbar\chi_w)(w - qA_\ell/\hbar c)$. Assuming that the current fulfills the

incompressible continuity equation $\partial_\ell j = 0$, we find that integrating the supercurrent along ℓ and applying Stokes' theorem yields

$$j = -\frac{c}{L}\oint \mathrm{d}\ell\, \delta_{A_\ell}\mathcal{F} = j_0(\mathcal{W}/2\pi - \Phi/\Phi_0), \tag{4}$$

where $j_0 \equiv 2\pi q/\hbar\chi_w L$ is the characteristic current, Φ is the externally applied magnetic flux $\Phi = \oint \mathrm{d}\ell\, A_\ell$, and $\Phi_0 = 2\pi\hbar c/q$ is the magnetic flux quantum [31,44,45]. The winding $\mathcal{W}$ and, hence, the current j depend on the spin texture, which is rooted in the bulk-edge correspondence of Eq. (2). Thus, $\mathcal{W}/4\pi$ can be understood as a fictitious skyrmion number. We will aim to use the magnetic flux Φ as a handle to control the supercurrent and trigger the nonsingular phase slip process, thereby driving skyrmion injection across the SQUID.

A. Adiabatic evolution

For a sufficiently slowly varying magnetic flux, the response of the spin texture and supercurrent may be well-approximated by the adiabatic evolution, which tracks the minimum of the free energy. Anticipating that the ground-state free-energy density is spatially homogeneous, we take an ansatz that the superconducting winding density w is constant, and the spin $\mathbf{s}$ uniformly sweeps out a cone l times around $\mathbf{z}$ as we move along ℓ, shown in Fig. 1. Such a texture $\{\mathbf{e}_1(\ell), \mathbf{e}_2(\ell), \mathbf{s}(\ell)\}$ can be constructed by starting with a uniform triad $\{\mathbf{x}, \mathbf{y}, \mathbf{z}\}$ and applying the ℓ-dependent rotation $R(\mathbf{z}, \varphi)R(\mathbf{y}, \theta)R(\mathbf{z}, \psi)$, where the Euler angles θ and $\varphi = 2\pi l\ell/L$ describe the polar and azimuthal angle of the spin texture $\mathbf{s}(\ell)$, respectively. In addition, $\psi = -2\pi(n+l)\ell/L$ corresponds to the intrinsic rotation of the triad around $\mathbf{s}(\ell)$. Then, the integrated winding is given by

$$\mathcal{W}(\theta) = 2\pi[n + l(1 - \cos\theta)], \tag{5}$$

so that n describes the multiples of 2π winding at $\theta = 0$. Sweeping θ from 0 to π injects l skyrmions across the one-dimensional loop, which facilitates a nonsingular phase slip of $4\pi l$.

Inserting the ansatz into the free energy of Eq. (3), we obtain $\mathcal{F}_{nl}(\Phi, \theta) = L_k j(\Phi, \theta)^2/2 + Jl^2 \sin^2\theta/2$. The dependence on Φ, n, and l enters through j from Eq. (4) and $\mathcal{W}$ from Eq. (5). Here, $L_k = \chi_w L\hbar^2/q^2$ is the kinetic inductance and $J = 4\pi^2 A/L$ is the characteristic exchange energy. Similarly, $L_k j_0^2$ is the characteristic superconducting winding energy. For this discussion, we focus on the winding-dominated limit $\kappa = J/L_k j_0^2 < 1$, which is also the stability condition for our ansatz. See Appendix C for a thorough analysis of the spin-triplet SQUID in the exchange-dominated $\kappa > 1$ regime.

In a more complete model, the magnetostatic energy must also be accounted for. The predominant contribution to this energy arises from the Oersted field produced by the supercurrent. This can be included in $\mathcal{F}_{nl}$ by the simple replacement $L_k \to L_k + L_g$, where L_g is the geometric inductance of the ring. Hence, the generated Oersted field favors the limit $\kappa < 1$. A less significant contribution is the magnetic field from the dipoles, which can be small compared to the Oersted field if the circumference L is much larger than the width of the ring [46].

B. Nonlinear response

Using the adiabatic evolution, the nonlinear response of the SQUID to the magnetic flux is determined by the ground-state spin texture θ_e, which fulfills $\partial_\theta \mathcal{F}_{nl}(\theta, \Phi)|_{\theta=\theta_e} = 0$ and $\partial_\theta^2 \mathcal{F}_{nl}(\theta, \Phi)|_{\theta=\theta_e} > 0$. This yields three potential solutions, $\theta_e = 0$, $\theta_e = \pi$, and

$$\theta_e = \cos^{-1}\left[\frac{n + l - \Phi/\Phi_0}{(1-\kappa)l}\right], \tag{6}$$

out of which only one is the unique ground state for a given value of n, l, and Φ. Once the equilibrium spin polar angle θ_e is determined for a given magnetic flux Φ, the supercurrent follows directly from Eq. (4).

As a concrete example (see Fig. 3), we initialize a system with $\Phi = 0$ (A) in the even topological sector with $\mathcal{W} = 0$ so that the ground state has zero supercurrent, $j = 0$, and the spin texture is uniformly aligned along $\mathbf{s}_0 = \mathbf{z}$ with $\theta_e = 0$. As the magnetic flux Φ is increased, negative supercurrent builds up as a diamagnetic response until it reaches the maximum value $-j^{\max} = -\kappa j_0$ at the critical flux $\kappa\Phi_0$ (B). Here, the spin texture with $\theta_e = 0$ becomes unstable. Upon further increasing Φ, it becomes energetically favorable to relax the supercurrent by changing the spin winding from $l = 0$ to $l = 1$ and to initiate a nonsingular phase slip; see Fig. 3(c). The polar angle θ_e sweeps from the north pole $\theta_e = 0$ (B) to the equator $\theta_e = \pi/2$ (C) to the south pole $\theta_e = \pi$ (D) [see Fig. 3(d)], whereupon the spin texture on the ring has traced out a full positive skyrmion charge at $(2-\kappa)\Phi_0$ [see Fig. 3(e)]. This completes a nonsingular 4π phase slip of the superconducting phase such that $\mathcal{W} = 4\pi$, bringing the supercurrent to $+j^{\max}$. Now, the diamagnetic response of the superconductor repeats until $-j^{\max}$ is reached at the critical value $(2+\kappa)\Phi_0$ (E). At this point, the sweeping reverses from $\theta_e = \pi$ to $\theta_e = 0$ (F) with a magnetic winding $l = -1$, which, again, traces out one full positive skyrmion charge at $(4-\kappa)\Phi_0$ [see Fig. 3(f)], engendering a second nonsingular 4π phase slip so that the winding becomes $\mathcal{W} = 8\pi$. This pattern repeats with periodicity $4\Phi_0$. We remark that without Zeeman or spin-orbit coupling, the free energy in Eq. (3) is invariant under global rotation of $\mathbf{s}$. Hence, the magnetic flux-induced switching can happen between arbitrary antipodal points $\mathbf{s}_0$ and $-\mathbf{s}_0$.

In the spin-triplet SQUID, the response of the supercurrent to the magnetic flux is nonlinear even without a Josephson junction, as seen in Fig. 3(b). While the electric current's sawtooth behavior [31] is reminiscent of the current response in the Little-Parks effect in U(1) superconductors [47], the current of the triplet superconductor relaxes continuously via nonsingular phase slips rather than singular phase slips. This gives rise to distinct falling and rising edge slopes, $-j^{\max}/\Phi_0\kappa$ and $j^{\max}/\Phi_0(1-\kappa)$, respectively, which, along with the $2\Phi_0$ periodicity in the magnetic flux [24,31], is an indicator of triplet superconductivity. Singular phase slip events, on the other hand, would relax the superconducting winding by 2π and are distinguishable from the nonsingular phase slips since they halve the flux periodicity to Φ_0 [31]. The supercurrent response could be measured by an inductively coupled tank circuit, operating analogously to the readout of the U(1) rf SQUID [31,48].

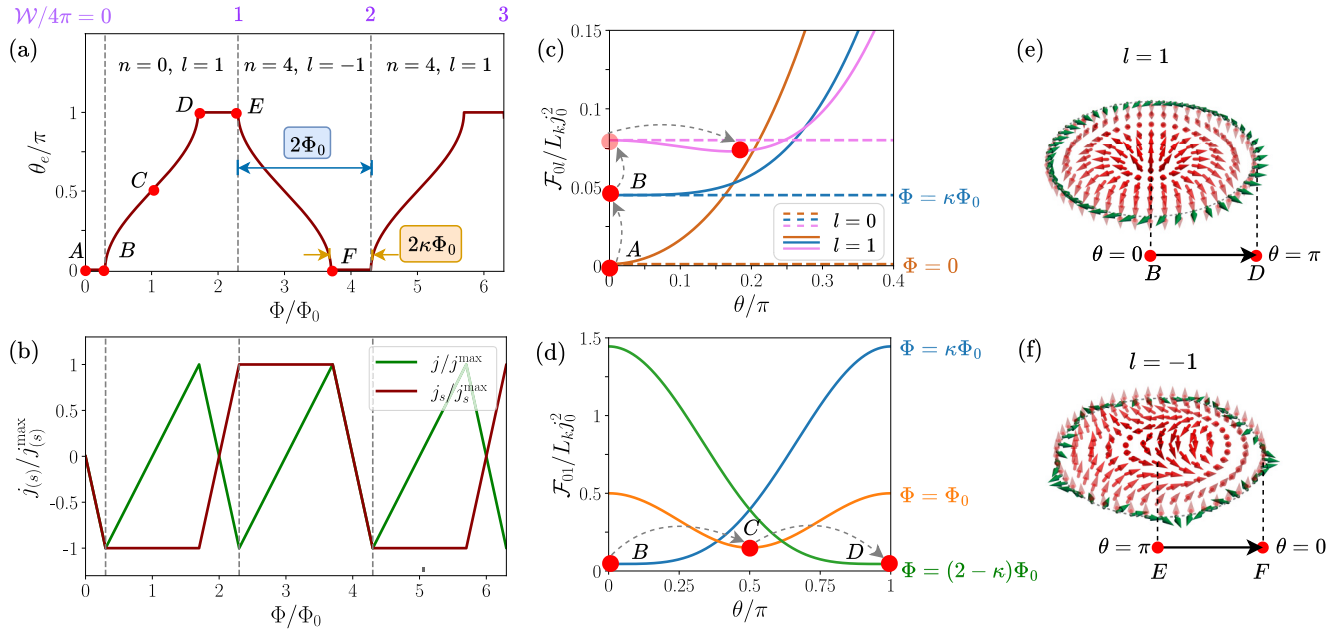

FIG. 3. (a) Plot of the energetic minimum θ_e as magnetic flux Φ is varied. Gray dashed lines indicate different integer values of 4π winding $\mathcal{W}$. (b) Plot of the normalized spin current $j_s/j_s^{\max}$ (red) and electric current $j/j^{\max}$ (green) as a function of Φ. (c) Depiction of switching from $\mathcal{F}_{00}$ to $\mathcal{F}_{01}$ as the critical magnetic flux $\kappa\Phi_0$ is reached. Dashed lines represent $\mathcal{F}_{00}(\Phi,\theta)$ and solid lines represent $\mathcal{F}_{01}(\Phi,\theta)$. (d) Evolution of the free energy $\mathcal{F}_{01}(\Phi,\theta)$ during the nonsingular phase slip. In (c) and (d), opaque red dots mark the ground state and the translucent red dot marks the unstable fixed point. (a)–(d) are plotted with $\kappa = 0.3$. (e) and (f) depict positive skyrmion charge swept out by the spin texture $\mathbf{s}$ (red arrows) on the ring as θ_e traverses from 0 to π and π to 0. (e) $l = 1$ spin winding; (f) $l = -1$ spin winding. Green arrows indicate the superconducting phase winding of $\mathbf{e}_1$ around $\mathbf{s}$ corresponding to (e) $\mathcal{W} = 4\pi$ and (f) $\mathcal{W} = 8\pi$.

Besides a charge supercurrent, the triplet superconductor also sustains a spin current $j_s = \hbar j s_z/q - A\mathbf{z}\cdot(\mathbf{s}\times\partial_\ell\mathbf{s})$ polarized in the z direction, where the first and second terms describe spin advection by the superflow and a spin current due to the noncollinear texture, respectively [49,50]. At equilibrium, the electric and spin currents are related by

$$j/j_s = (q/\hbar)\cos\theta_e, \tag{7}$$

which follows from Eqs. (4)–(6) and holds for all values of Φ. We find that the spin current exhibits an oscillatory behavior with periodicity $4\Phi_0$, twice that of the supercurrent; see Fig. 3(b). Furthermore, the spin current is at a maximal value of $\pm\hbar j^{\max}/q$ during the nonsingular phase slip and changes values only when the spin texture is collinear.

IV. DISSIPATION

For a more complete treatment, we include dissipation of the triplet superconductor due to, e.g., Gilbert damping and Joule heating of the normal electrons. To this end, we choose the noncanonical degrees of freedom, $\mathbf{X} = \{\rho, \mathbf{s}, w\}$, where we have reincluded the charge density ρ to account for both superconducting and normal electrons. When constructing the equations of motion, we must make sure that the dissipative terms preserve $\delta\mathcal{W} = \int \mathrm{d}t \oint \mathrm{d}\ell\, j_{\mathrm{sk}}$, which is rooted in the topological bulk-edge correspondence. Furthermore, they must maintain the spin length, $\mathbf{s}^2 = 1$, and obey charge conservation. To this end, we propose a variant of Hamilton's equations [51,52],

$$\dot{X}_i(\ell,t) = \sum_j \int \mathrm{d}\ell' \{X_i(\ell,t), X_j(\ell',t)\}\mathfrak{F}_j(\ell',t). \tag{8a}$$

Here, we have defined the generalized force,

$$\mathfrak{F} \equiv \delta_{\mathbf{X}}\mathcal{F}[\mathbf{X}] + \delta_{\dot{\mathbf{X}}}\mathcal{R}[\dot{\mathbf{X}}], \tag{8b}$$

to be the sum of the nondissipative force stemming from the free energy $\mathcal{F}$ and the dissipative force, which is derived from the Rayleigh functional $\mathcal{R}$. The latter is constructed in accordance with the second law of thermodynamics and Onsager reciprocity.

Formally, the structural invariants detailed above correspond to Casimir invariants. Remarkably, Eq. (8) will maintain all such Casimir invariants for a generic Rayleigh functional $\mathcal{R}[\dot{\mathbf{X}}]$ constructed from velocities $\dot{\mathbf{X}}$. In contrast, a dissipation functional $\mathcal{R}[\delta_{\mathbf{X}}\mathcal{F}]$ constructed from thermodynamic forces $\delta_{\mathbf{X}}\mathcal{F}$ [52] may no longer conserve these Casimir invariants [53]. The details of this construction are discussed thoroughly in Appendix D.

Once the Poisson brackets, the free energy, and the Rayleigh functional are specified, the equations of motion naturally follow. To derive the Poisson brackets, we first assume zero temperature and use $\{d_i^*(\ell), d_j(\ell')\} = i\delta_{ij}\delta(\ell-\ell')/\hbar$ and $\{d_i(\ell), d_j(\ell')\} = 0$ [24], which can be motivated from a microscopic theory; see Appendix E. We find

[24,54]

$$\{s_i(\ell), s_j(\ell')\} = \epsilon_{ijk} s_k \delta(\ell - \ell')/s, \tag{9a}$$

$$\{w(\ell), \rho(\ell')\} = -q\partial_\ell \delta(\ell - \ell')/\hbar, \tag{9b}$$

$$\{w(\ell), \mathbf{s}(\ell')\} = q\partial_\ell \mathbf{s}\, \delta(\ell - \ell')/\hbar\rho, \tag{9c}$$

where all other Poisson brackets of ρ, $\mathbf{s}$, and w evaluate to zero. Here, we have used the zero-temperature identification of $s = \hbar d^2$ as the saturated spin density and $\rho = qd^2$ as the charge density. However, we expect these results to qualitatively hold for finite temperatures, where s and ρ are promoted to total spin and charge densities, respectively, and include both normal and superconducting contributions. For a fully spin-polarized superconductor, we retain the relation $s = \hbar\rho/q$. The nuances of this generalization are discussed in detail in the last paragraph of Appendix E. Equation (9a) is the usual spin algebra, Eq. (9b) establishes the charge density as the generator of phase rotations, identically to a U(1) superconductor, and Eq. (9c) captures the linkage between superconducting winding and spin texture.

The free energy is given by Eq. (3), with the addition of the nonelectrostatic contribution $\int \mathrm{d}\ell\, (\rho - \rho_0)^2/2\chi_c$, where χ_c is the charge compressibility. In the Weyl gauge, the electrostatic contribution is absent and the nonelectrostatic contribution captures small fluctuations of ρ away from the equilibrium charge density ρ_0. Moreover, the Rayleigh functional is constructed from the gauge-independent velocities $\partial_t \mathbf{s}$ and $\partial_t(w - qA_\ell/\hbar c)$,

$$\mathcal{R} = \int \mathrm{d}\ell \left\{ \frac{\alpha s}{2} (\partial_t \mathbf{s})^2 + \frac{\sigma}{2} \left[\partial_t \left(\frac{\hbar w}{q} - \frac{A_\ell}{c} \right) \right]^2 \right\}. \tag{10}$$

The first term corresponds to Gilbert damping with damping coefficient α and the second term describes Joule heating with conductivity σ. Using Eqs. (8)–(10), the equations of motion are

$$\partial_t \rho = -\partial_\ell \mathfrak{J}, \tag{11a}$$

$$\partial_t \mathbf{s} = \mathbf{s} \times \mathbf{H}_{\mathrm{eff}} - \alpha \mathbf{s} \times \partial_t \mathbf{s} - \mathfrak{J} \partial_\ell \mathbf{s}/\rho, \tag{11b}$$

$$\partial_t w = -q\partial_\ell \mu/\hbar + j_{\mathrm{sk}}, \tag{11c}$$

and have been written using the constitutive relation

$$\mathfrak{J} = j + \sigma \mathcal{E}, \quad \text{where} \quad \mathcal{E} = E_\ell - \partial_\ell \mu + \hbar j_{\mathrm{sk}}/q. \tag{12}$$

Here, $\mathbf{H}_{\mathrm{eff}} = -\delta_{\mathbf{s}} \mathcal{F}/s$ is the effective magnetic field and $\mu = \delta_\rho \mathcal{F}$ is the chemical potential. The equations of motion describe the charge continuity equation in Eq. (11a), the Landau-Lifshitz-Gilbert equation in Eq. (11b), and the rate of change of winding in Eq. (11c) which corresponds to the spin-triplet version of the first London equation [25]. From the charge continuity equation (11a), $\mathfrak{J} = -c\delta_{A_\ell} \mathcal{F} - c\delta_{\dot{A}_\ell} \mathcal{R}$ is identified as the total charge current, which is driven by the electromotive force $\mathcal{E}$. The latter has contributions from the electric field $E_\ell = -\partial_t A_\ell/c$, the gradient of μ, and the motive force due to a transverse skyrmion flux directed towards the center of the loop, j_{sk}. Furthermore, the motive force from j_{sk} is Onsager reciprocal to the adiabatic spin-transfer torque on the spin orientation $\mathbf{s}$; see Eq. (11b) [55,56]. Remarkably, there is no term in either the free energy or the Rayleigh function that couples the spin texture and the charge current. Rather, these cross couplings appear due to the nontrivial Poisson bracket in Eq. (9c), which encodes the advection of spin by the superflow [52,54]. Finally, the equations of motion can be straightforwardly generalized to three dimensions (3D); see Appendix F.

In this construction, the topological relation $\delta\mathcal{W} = \int \mathrm{d}t \oint \mathrm{d}\ell\, j_{\mathrm{sk}}$ holds even in the presence of dissipation. This can be seen by integrating Eq. (11c) along the 1D loop. Moreover, freezing out magnetic dynamics so that $j_{\mathrm{sk}} = 0$ restores the conservation of superconducting winding, i.e., winding satisfies the continuity equation $\partial_t w = -\partial_\ell j_w$. Here, the winding flux is given by $j_w = -\mathbf{e}_1 \cdot \partial_t \mathbf{e}_2$ and can be identified with $q\partial_\ell \mu/\hbar$ upon comparison with Eq. (11c). On the other hand, if $j_{\mathrm{sk}} \neq 0$, the magnetic dynamics can induce nonsingular phase slips in the winding, which is the key mechanism used in the SQUID device. We note that in 2D and 3D spin-triplet superconductors, the natural topological charge carriers are skyrmions and hopfions, respectively, as discussed in Appendix G.

Finally, a linearized analysis of Eqs. (11) confirms the stability of our ansatz for adiabatic evolution in the $\kappa < 1$ regime. In contrast, for the $\kappa > 1$ regime, the texture discontinuously switches between the antipodal fixed points $\pm\mathbf{s}_0$, and the current exhibits a sawtooth response. Furthermore, in both regimes, the onset of instability of the collinear spin texture coincides with the initiation of the nonsingular phase slip. The details of this linearized analysis are presented in Appendix H.

V. DISCUSSION

Our work scaffolds a conceptual framework for understanding the phenomena that arise when the U(1) order parameter space of a superconductor is enriched. For the example of a fully spin-polarized triplet superconductor, we found that the topological structure of the SO(3) order parameter space is reflected by the bulk-edge correspondence of Eq. (2), which facilitates topological hydrodynamics of magnetic skyrmions that are inherently tied to the superconducting winding. Continuously moving a skyrmion through a loop engenders a nonsingular phase slip, signifying the passage of a coreless vortex [30]. To motivate future experiments and technologies, we leveraged this physics to devise the spin-triplet SQUID, which functions without a Josephson weak link.

Similar physics can arise in dipole-locked ^{3}He-A, which has an SO(3) order parameter intertwining orbital angular momentum with phase winding [4,40,57–59]. By analogy to the spin-triplet SQUID, nonsingular phase slips could be used in a superfluid ^{3}He-A quantum interference device (SHeQUID). While current versions of the SHeQUID are based on ^{4}He and ^{3}He-B and function with singular phase slips [60], nonsingular phase slips could obviate the need for a Josephson weak link, while still allowing a rotation sensor modality. Moreover, based on general symmetry grounds, we expect that a similar phenomenological theory describes superfluids in which phase winding coexists with a local angular momentum density. Namely, Eqs. (8)–(12) are valid independent of the SO(3)-specific Mermin-Ho constraint; see Eq. (2). The latter is encoded by the initial conditions and preserved by the equations of motion. For example, our theory might apply to

the β phase of ^{3}He [61] or to spin-polarized triplet excitonic insulators, the latter of which may have been experimentally realized in Ref. [62].

For future works, a similar analysis could also be applied to other enriched superconducting order parameter spaces $\mathcal{M}$. Borrowing the language of algebraic topology, we conjecture that coreless vortices are allowed if $\pi_2[\mathcal{M}, \mathrm{U}(1)]/\ker\partial = \mathbb{Z}$; see Appendix B [37]. Here, $\ker\partial$ is a subgroup of $\pi_2[\mathcal{M}, \mathrm{U}(1)]$ classifying topological defects that have *zero phase winding* around the boundary, but a potentially nontrivial $\mathcal{M}$ texture in the bulk. Modding out such bulk textures, the quotient group classifies the remaining nonsingular textures via the boundary winding. This allows for a bulk-edge correspondence that gives rise to topological hydrodynamics of coreless vortices that can initiate nonsingular phase slips.

ACKNOWLEDGMENTS

This work is supported by NSF under Grant No. DMR-2049979. B.B. acknowledges support from the Research Council of Norway through the Centres of Excellence funding scheme, Project No. 262633, "QuSpin." C.D. and E.K. thank Shane P. Kelly for many fruitful discussions.

DATA AVAILABILITY

There are no publicly available research data or software supporting this manuscript. Requests for further information or data should be sent to the authors.

APPENDIX A: ORDER PARAMETER

We are interested in smoothly varying textures of an SO(3) order parameter that is described by the complex vector field [23,25,63,64]

$$\mathbf{d}(\mathbf{r}) = \frac{d(\mathbf{r})}{\sqrt{2}} e^{i\phi(\mathbf{r})}[\mathbf{e}_1(\mathbf{r}) + i\,\mathbf{e}_2(\mathbf{r})], \tag{A1}$$

where $\phi(\mathbf{r})$ is the superconducting phase, $d(\mathbf{r}) = \sqrt{\mathbf{d}^*\cdot\mathbf{d}}$ is the modulus of the order parameter, and the real vectors $\mathbf{e}_1$ and $\mathbf{e}_2$ are orthonormal, $\mathbf{e}_a\cdot\mathbf{e}_b = \delta_{ab}$. From the order parameter, we can derive the hydrodynamic variables spin orientation $\mathbf{s}$ and superconducting winding $\mathbf{w}$ via

$$\mathbf{s} = \frac{i\mathbf{d}\times\mathbf{d}^*}{d^2} = \mathbf{e}_1\times\mathbf{e}_2 \tag{A2}$$

and

$$w_i = \frac{1}{2id^2}(\mathbf{d}^*\cdot\partial_i\mathbf{d} - \mathbf{d}\cdot\partial_i\mathbf{d}^*) = \partial_i\phi + \mathbf{e}_1\cdot\partial_i\mathbf{e}_2, \tag{A3}$$

where the second term takes the role of a connection. For generality, we consider 3D with $i \in \{x, y, z\}$, noting that the 1D and 2D cases follow straightforwardly.

Importantly, the $\mathbf{d}$ vector fulfills the residual symmetry

$$e^{i\chi}R(\mathbf{s}, \chi)\mathbf{d} = \mathbf{d}, \tag{A4}$$

that is, a combination of a local phase transformation with a commensurate local rotation around $\mathbf{s}$ leaves the order parameter unchanged. This has been used in Sec. II in order to make the gauge choice of $\phi = 0$, so that the triad $\{\mathbf{e}_1, \mathbf{e}_2, \mathbf{s}\}$ fully captures the orientational degrees of freedom and the winding $\mathbf{w}$ is identified with the connection in Eq. (1).

Assuming the order parameter does not vanish anywhere, $d \neq 0$, we obtain the Mermin-Ho relation,

$$(\nabla\times\mathbf{w})_k = \frac{\epsilon_{ijk}}{2}\mathbf{s}\cdot(\partial_i\mathbf{s}\times\partial_j\mathbf{s}), \tag{A5}$$

where the term on the right-hand side is the skyrmion density.

Formally, the emergence of an $\mathcal{M} = \mathrm{SO}(3)$ order parameter space can be discussed via spontaneous symmetry breaking [24,57]. To this end, we assume that the free energy is invariant under $G = \mathrm{SO}(3)_\mathbf{s}\times\mathrm{U}(1)_\phi$ describing $\mathrm{SO}(3)_\mathbf{s}$ spin rotations and $\mathrm{U}(1)_\phi$ phase transformations. Assuming negligible spin-orbit coupling, orbital degrees of freedom are disregarded. In the fully spin-polarized triplet state, the total symmetry G is broken, but we maintain the residual symmetry $H = \mathrm{U}(1)_{s_z+\phi}$ of joint spin rotations and phase transformations, captured by Eq. (A4). Thus, the order parameter space is given by

$$\mathcal{M} = G/H = \frac{\mathrm{SO}(3)_\mathbf{s}\times\mathrm{U}(1)_\phi}{\mathrm{U}(1)_{s_z+\phi}} = \mathrm{SO}(3)_{\mathbf{s},\phi}. \tag{A6}$$

This symmetry analysis is similar to that done for the A phase of superfluid ^{3}He [57].

APPENDIX B: CORELESS VORTICES

Enriching the order parameter in superconductors from U(1) to $\mathcal{M} \supset \mathrm{U}(1)$ can give rise to interesting topological hydrodynamics. In particular, it allows for coreless vortices that can trigger nonsingular phase slips. The spin-triplet skyrmions studied in the main text are examples of such coreless vortices for $\mathcal{M} = \mathrm{SO}(3)$. In general, to predict if an enriched superconductor is capable of hosting such coreless vortices in two dimensions, we use the *relative* homotopy $\pi_2[\mathcal{M}, \mathrm{U}(1)]$ [37], which studies homotopy classes of maps $(D^2, \partial D^2) \to [\mathcal{M}, \mathrm{U}(1)]$, where D^2 is the two-dimensional disk and ∂D^2 its boundary. The long exact sequence of group homorphisms provides a useful tool to relate the relative homotopy $\pi_2[\mathcal{M}, \mathrm{U}(1)]$ to the better-known bulk homotopy $\pi_2(\mathcal{M})$ and edge homotopy $\pi_1[\mathrm{U}(1)]$,

$$\cdots \to \pi_2(\mathcal{M}) \xrightarrow{j_*} \pi_2[\mathcal{M}, \mathrm{U}(1)] \xrightarrow{\partial} \pi_1[\mathrm{U}(1)] \to \cdots. \tag{B1}$$

The first group homomorphism j_* is constructed by viewing the absolute maps $S^2 \to \mathcal{M}$ of $\pi_2(\mathcal{M})$ as relative maps $(D^2, \partial D^2) \to (\mathcal{M}, x_0)$ of $\pi_2[\mathcal{M}, \mathrm{U}(1)]$, where the boundary ∂D^2 is collapsed to the basepoint $x_0 \in \mathrm{U}(1)$. The second group homomorphism is the boundary map ∂, which simply ignores the $\mathcal{M}$ texture in the bulk and outputs the homotopic classification of the U(1) texture on the edge. As the sequence is exact, it is guaranteed that $\mathrm{im}\, j_* = \ker\partial$. Importantly, we can understand $\mathrm{im}\, j_*$ and $\ker\partial$ as the subgroup of $\pi_2[\mathcal{M}, \mathrm{U}(1)]$ classifying topological defects that have *zero phase winding* around the boundary, but a potentially nontrivial $\mathcal{M}$ texture in the bulk.

Now, we are equipped to formulate our conjecture for the existence of coreless vortices. In other words, we want to prove the existence of two-dimensional topological defects classified by $\pi_2[\mathcal{M}, \mathrm{U}(1)]$ that fulfill a bulk-edge correspondence. Namely, they are classified by $\pi_1[\mathrm{U}(1)]$ on the edge of the disk. To quotient out the edge-independent bulk topological defects described by $\mathrm{im}\, j_*$, we suggest that the

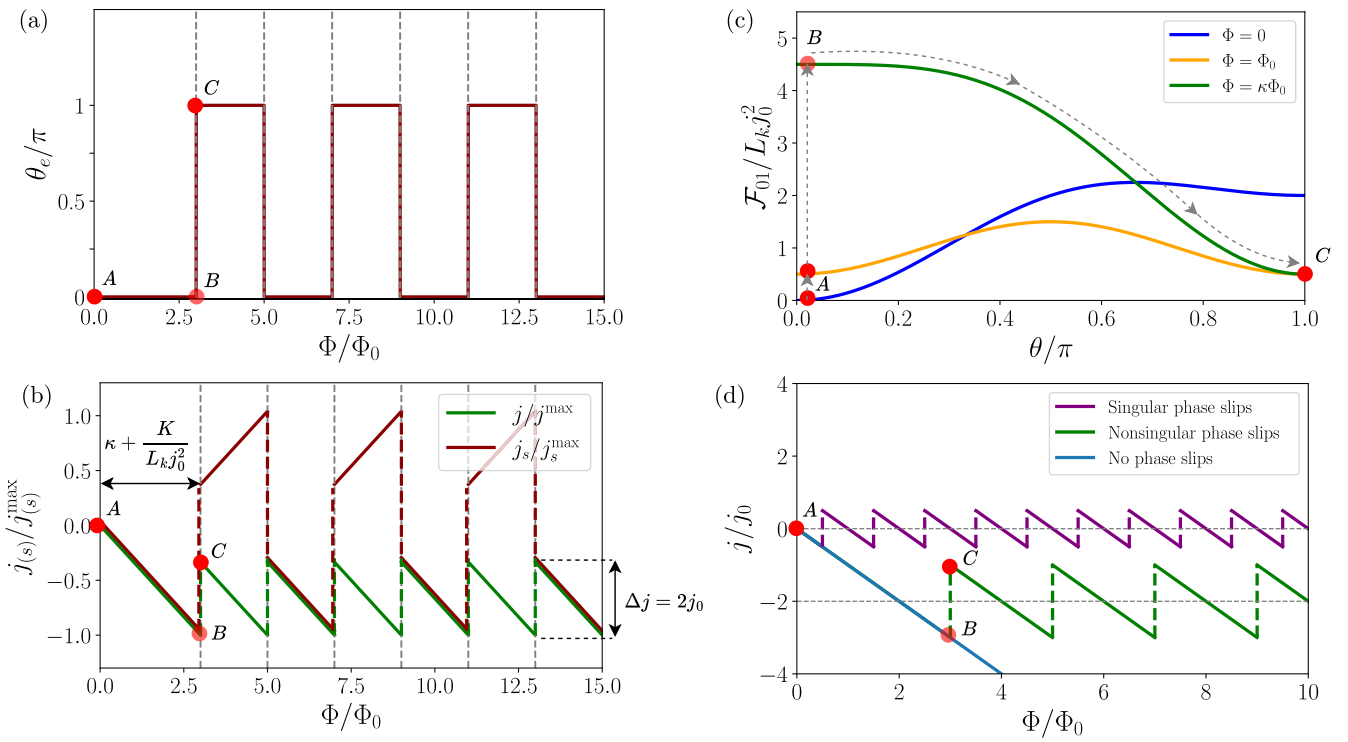

FIG. 4. Magnetic and current response of the spin-triplet SQUID in the $\kappa > 1$ regime. (a) and (b) are plotted for $\kappa = 3$ and $K/L_k j_0^2 = 0$. (c) The free-energy landscape during the nonsingular phase slip in the $\kappa > 1$ regime, where $\mathcal{F}_{nl}(\theta, \Phi)$ is identical to the definition used in the main text. Opaque red dots mark the stable fixed point and the translucent red dot marks the unstable fixed point. (d) Current response to a magnetic flux, contrasting the case of singular phase slips, nonsingular phase slips, and no phase slips allowed. The purple and green dashed lines indicate discontinuous jumps of the current.

criterion is

$$\pi_2[\mathcal{M}, \mathrm{U}(1)]/\mathrm{im}\, j_* \cong \mathbb{Z}. \tag{B2}$$

If the integer numbers $\mathbb{Z}$ survive this group quotient, there are coreless vortices that can be extensively built up. This can be further shown by using $\mathrm{im}\, j_* = \ker \partial$ and the group isomorphism $\pi_2[\mathcal{M}, \mathrm{U}(1)]/\ker \partial \cong \mathrm{im}\, \partial$. Note that the latter is simply an application of the fundamental theorem on group homomorphisms. Then, we can define the more refined conjecture that for

$$\mathrm{im}\, \partial = n\,\mathbb{Z} \leqslant \pi_1[\mathrm{U}(1)], \tag{B3}$$

with $n = \{1, 2, \ldots\}$, the superconductor can host coreless vortices with elementary topological charge of $\pm 2\pi n$ winding. For a given n, a finite winding $\mathcal{W} \in 2\pi\, n\,\mathbb{Z}$ on the boundary can be realized by coreless vortices in the bulk. In order to evaluate $\mathrm{im}\, \partial$, it might be helpful to extend the long exact sequence via $\pi_1[\mathrm{U}(1)] \xrightarrow{i_*} \pi_1(\mathcal{M}) \to \cdots$, where i_* is the induced map from the inclusion $i : \mathrm{U}(1) \hookrightarrow \mathcal{M}$. Then, we can use that $\mathrm{im}\, \partial = \ker i_*$ and evaluate the latter. Hence, the question becomes: Which loops with winding $\mathcal{W} \in 2\pi\, \mathbb{Z}$ in U(1) become trivial when included in the enriched order parameter space $\mathcal{M}$?

For the case of a fully polarized spin-triplet superconductor with $\mathcal{M} = \mathrm{SO}(3)$, we have no nontrivial bulk topological defects in two dimensions, $\pi_2[\mathrm{SO}(3)] = 0$, but the relative homotopy is $\pi_2[\mathrm{SO}(3), \mathrm{U}(1)] = \mathbb{Z}$ (following from $\pi_2[\mathrm{SO}(3), \mathrm{U}(1)] = \pi_2(S^2)$ through fibration [37]). Hence, the group quotient by $\mathrm{im}\, j_* = 0$ yields

$$\pi_2[\mathrm{SO}(3), \mathrm{U}(1)]/\mathrm{im}\, j_* \cong \mathbb{Z}. \tag{B4}$$

We conclude that spin-triplet superconductors can host coreless vortices that can be extensively built up. By studying the induced inclusion map i_* from $\pi_1[\mathrm{U}(1)] = \mathbb{Z}$ to $\pi_1[\mathrm{SO}(3)] = \mathbb{Z}_2$, we infer that only even winding numbers become trivial under inclusion, $\ker i_* = 2\mathbb{Z}$. Hence, with Eq. (B3), the elementary topological charge of these coreless vortices is $\pm 4\pi$, in accordance with the spin-triplet skyrmions studied in the main text.

APPENDIX C: SQUID ANALYSIS IN EXCHANGE-DOMINATED REGIME

Here, we discuss the exchange-dominated $\kappa > 1$ regime of the SQUID. For the energetic analysis, we use the free energy of the 1D ring

$$\mathcal{F}_{nl}(\Phi, \theta) = \frac{1}{2} L_k j(\Phi, \theta)^2 + \frac{1}{2} J l^2 \sin^2\theta - \frac{K}{2}\cos^2\theta, \tag{C1}$$

where we added the easy-axis anisotropy term with $K > 0$ and $j(\Phi, \theta) = j_0[n + l(1 - \cos\theta) - \Phi/\Phi_0]$ is the current evaluated from Eqs. (4) and (5). In contrast to the winding-dominated $\kappa < 1$ regime discussed in Sec. III, the only stable (or metastable) states are collinear with $\theta_e = 0$ or $\theta_e = \pi$. Hence, the magnetic texture exhibits a square wave response, switching discontinuously between these two states, which is reflected in Fig. 4(a).

In Figs. 4(a)–4(c), we initialize the system so that the spin texture is collinear with $\theta_e = 0$ and the magnetic flux as well as the current is zero (A). As the magnetic flux is increased, the current shows a diamagnetic response; see Fig. 4(b). The collinear spin texture with $\theta_e = 0$ stays stable up until $\Phi = \Phi_0$, where the texture becomes metastable; see Fig. 4(c). Then, at the critical flux value (B) of

$$\Phi_c = \left(\kappa + \frac{K}{L_k j_0^2}\right)\Phi_0, \tag{C2}$$

the texture becomes unstable. At this point, the current reaches $-j^{\max}$, with the maximal magnitude given by

$$j^{\max} = j_0 \Phi_c/\Phi_0 = j_0\left(\kappa + \frac{K}{L_k j_0^2}\right); \tag{C3}$$

see Fig. 4(b). Here, the easy-axis anisotropy K stabilizes the collinear spin texture, thus requiring a higher magnetic flux, and hence a higher maximal current, before we reach an instability.

Once the collinear spin texture with $\theta_e = 0$ destabilizes (B), a "runaway" nonsingular phase slip initiates ($B \to C$), during which the magnetic texture passes through a skyrmion and switches to the new ground-state magnetic texture at $\theta_e = \pi$ (C); see Fig. 4(c). As a result, the current relaxes (increases) by

$$\Delta j = 2 j_0 l_*, \tag{C4}$$

where l_* is the absolute value of the spin winding. For $K = 0$, an energetic analysis suggests that $l_* = 1$ and, for $K \neq 0$, we find that l_* satisfies $l_*(l_* - 1) < K/J < l_*(l_* + 1)$. Hence, during the nonsingular phase slip, the magnetic texture "passes through" l_* number of skyrmions to lower the free energy. Further increasing the magnetic flux, the diamagnetic response decreases the current back to $-j^{\max}$, whereupon the process repeats with periodicity $2\Phi_0 l_*$. For $l_* = 1$, the periodicity is the same as in the main text.

Since the spin texture is always collinear, the spin current stems entirely from spin advection by the superflow. In Fig. 4(b), the spin current (red line) is given by $j_s = \pm\hbar j/q$, where the sign depends on θ_e; see Eq. (7).

Finally, we discuss the charge current response of the triplet superconductor when singular phase slips are also allowed; see Fig. 4(d). Without either singular or nonsingular phase slips, the diamagnetic current response is linear (blue line). By including the nonsingular phase slips (green line), the average current (dashed line) is nonzero, as it can only relax by Δj once it becomes energetically preferred to distort the spin texture to pass through skyrmion charge. In contrast, if singular phase slips are allowed (purple line), the average current becomes zero. In addition, the periodicity is reduced from $2\Phi_0 l_*$ to Φ_0 as is Δj from $2 j_0 l_*$ to j_0.

APPENDIX D: DISSIPATION

Here, we describe how dissipation can be included in the equations of motion while still maintaining certain topological constraints encoded in Casimir invariants. For a noncanonical system of fields $\mathbf{X} = \{X_1, X_2, \ldots\}$, we can describe the nondissipative dynamics using Hamilton's equation,

$$\dot{X}_i(\mathbf{r}, t) = \{X_i(\mathbf{r}, t), \mathcal{F}\} = \int \mathrm{d}V' J_{ij}(\mathbf{r}, \mathbf{r}') \frac{\delta \mathcal{F}}{\delta X_j(\mathbf{r}', t)}, \tag{D1}$$

where we consider 3D with $\mathbf{r} = (x, y, z)$. The 1D and 2D equations follow analogously. From here on, we assume the convention of Einstein summation over repeated indices. We also introduce the Poisson operator as $J_{ij}(\mathbf{r}, \mathbf{r}') \equiv \{X_i(\mathbf{r}, t), X_j(\mathbf{r}', t)\}$ and $\mathcal{F}[\mathbf{X}]$ is the free-energy functional.

1. Casimir invariants

We stress that once the fields $\mathbf{X}$ and their Poisson brackets are defined, noncanonical Poisson brackets can give rise to Casimir invariants $\mathcal{Q}$. We distinguish between local Casimir invariants $\mathcal{Q}(\mathbf{r})$ given by a local function of the fields $\mathbf{X}$ at point $\mathbf{r}$ and global (or integrated) Casimir invariants $\mathcal{Q}[\mathbf{X}]$ given by a functional. Local Casimir invariants fulfill

$$\begin{aligned}\dot{\mathcal{Q}}(\mathbf{r}) &= \{\mathcal{Q}(\mathbf{r}), \mathcal{F}\} \\ &= \int \mathrm{d}V' \int \mathrm{d}V'' \frac{\delta \mathcal{Q}(\mathbf{r})}{\delta X_i(\mathbf{r}', t)} J_{ij}(\mathbf{r}', \mathbf{r}'') \frac{\delta F}{\delta X_j(\mathbf{r}'', t)} = 0,\end{aligned} \tag{D2}$$

for arbitrary free-energy functionals $\mathcal{F}$. This requires

$$\{\mathcal{Q}(\mathbf{r}), X_j(\mathbf{r}'')\} = \int \mathrm{d}V' \frac{\delta \mathcal{Q}(\mathbf{r})}{\delta X_i(\mathbf{r}', t)} J_{ij}(\mathbf{r}', \mathbf{r}'') = 0, \tag{D3}$$

which immediately yields zero in Eq. (D2). Hence, whenever such Casimir invariants exist, the Poisson operator $J_{ij}(\mathbf{r}, \mathbf{r}')$ has a finite kernel, and hence, $J_{ij}(\mathbf{r}, \mathbf{r}')$ in Eq. (D1) cannot be inverted. This will become crucial when we include dissipation below. Global Casimir invariants, on the other hand, fulfill the weaker version of a conservation law,

$$\begin{aligned}\dot{\mathcal{Q}}[\mathbf{X}] &= \{\mathcal{Q}[\mathbf{X}], \mathcal{F}\} \\ &= \int_{\mathcal{A}} \mathrm{d}V' \int_{\mathcal{A}} \mathrm{d}V'' \frac{\delta \mathcal{Q}[\mathbf{X}]}{\delta X_i(\mathbf{r}', t)} J_{ij}(\mathbf{r}', \mathbf{r}'') \frac{\delta \mathcal{F}}{\delta X_j(\mathbf{r}'', t)} = I_{\mathcal{Q}}|_{\partial \mathcal{A}},\end{aligned} \tag{D4}$$

where we allow a current $I_{\mathcal{Q}}|_{\partial \mathcal{A}}$ at the boundary $\partial \mathcal{A}$ of some region $\mathcal{A}$. This conservation law holds for arbitrary free energies $\mathcal{F}$ if

$$\begin{aligned}\{\mathcal{Q}[\mathbf{X}], X_j(\mathbf{r}'')\} &= \int \mathrm{d}V' \frac{\delta \mathcal{Q}[\mathbf{X}]}{\delta X_i(\mathbf{r}', t)} J_{ij}(\mathbf{r}', \mathbf{r}'') \\ &= \int \mathrm{d}V' \nabla' \cdot \mathbf{K}_j(\mathbf{r}', \mathbf{r}''),\end{aligned} \tag{D5}$$

for some local vector kernel $\mathbf{K}_j(\mathbf{r}', \mathbf{r}'')$. For this vector kernel, we can define $\mathbf{j}_{\mathcal{Q}}(\mathbf{r}) \equiv -\int_{\mathcal{A}} \mathrm{d}V' \mathbf{K}_j(\mathbf{r}, \mathbf{r}') \frac{\delta \mathcal{F}}{\delta X_j(\mathbf{r}', t)}$ as the current density, for which we find that $I_{\mathcal{Q}}|_{\partial \mathcal{A}} = -\int_{\mathcal{A}} \mathrm{d}V \nabla \cdot \mathbf{j}_{\mathcal{Q}}(\mathbf{r})$. We stress that both local and global Casimir charges $\mathcal{Q}$ derive from the Poisson brackets rather than from symmetries of the free energy $\mathcal{F}$. Thus, they are distinct from conserved Noether charges.

As a first educational example of a local Casimir invariant, we consider a magnet with $\mathbf{X} = \{s_x, s_y, s_z\}$ describing the spin orientation $\mathbf{s}$ with constant spin density s. The noncanonical Poisson brackets fulfill $J_{ij}(\mathbf{r}, \mathbf{r}') = \{s_i(\mathbf{r}), s_j(\mathbf{r}')\} = \epsilon_{ijk} s_k \delta(\mathbf{r} - \mathbf{r}')/s$, which generates the equation of motion,

$\dot{\mathbf{s}} = -\mathbf{s} \times \delta_{\mathbf{s}}\mathcal{F}/s$. For the local Casimir invariant $\mathcal{Q} = \mathbf{s}^2$, one can easily verify Eq. (D3). Hence, $\mathcal{Q}$ is conserved regardless of the free energy $\mathcal{F}$.

As a second educational example of a global Casimir invariant, we consider a superconductor with $\mathbf{X} = \{\rho, \mathbf{w}\}$ describing the charge density ρ and the winding density $\mathbf{w}$ of the superconducting phase. The Poisson brackets are given by $\{w_i(\mathbf{r}), \rho(\mathbf{r}')\} = -q\partial_i\delta(\mathbf{r} - \mathbf{r}')/\hbar$. For the global Casimir invariant $\mathcal{Q} = \int \mathrm{d}V\,\rho$ (total charge), we can immediately verify Eq. (D5), where $\mathbf{K}_j(\mathbf{r}', \mathbf{r}'') = q\,\mathbf{e}_j\delta(\mathbf{r}' - \mathbf{r}'')/\hbar$. In its local form, we obtain the continuity equation $\dot{\rho} = -q\boldsymbol{\nabla} \cdot \delta_{\mathbf{w}}\mathcal{F}/\hbar$. Thus, by construction, charge is conserved up to boundary terms, where a current can be injected.

2. $\mathcal{Q}$-conserving dissipation

For dissipation to conserve the Casimir invariants $\mathcal{Q}$, we propose the following equations of motion:

$$\dot{X}_i(\mathbf{r}, t) = \int \mathrm{d}V' J_{ij}(\mathbf{r}, \mathbf{r}') \left[\frac{\delta\mathcal{F}[\mathbf{X}]}{\delta X_j(\mathbf{r}', t)} + \frac{\delta\mathcal{R}[\dot{\mathbf{X}}]}{\delta\dot{X}_j(\mathbf{r}', t)} \right], \quad \text{(D6)}$$

where the Rayleighian is constructed as a bilinear functional of the velocities,

$$\mathcal{R}[\dot{\mathbf{X}}] = \int \mathrm{d}V \int \mathrm{d}V' \frac{1}{2} \dot{X}_i(\mathbf{r}, t) R_{ij}(\mathbf{r}, \mathbf{r}') \dot{X}_j(\mathbf{r}', t). \quad \text{(D7)}$$

Here, $R_{ij}(\mathbf{r}, \mathbf{r}') = R_{ji}(\mathbf{r}', \mathbf{r})$ is a local kernel that can depend on the fields $\mathbf{X}$. Note that by construction, the dissipation in Eq. (D6) cannot violate the conservation of Casimir invariants $\mathcal{Q}$ as long as either Eq. (D3) or Eq. (D5) is fulfilled.

Coming back to our example of the magnet, any Rayleighian constructed from velocities $\mathcal{R} = \mathcal{R}[\dot{\mathbf{s}}]$ (for example, Gilbert damping) will generate the equations of motion, $\dot{\mathbf{s}} = -\mathbf{s} \times (\delta_{\mathbf{s}}\mathcal{F} + \delta_{\dot{\mathbf{s}}}\mathcal{R})/s$, where it can be easily seen that the local Casimir invariant $\mathcal{Q} = \mathbf{s}^2$ is still conserved.

Similarly, for the example of the superconductor, any Rayleighian $\mathcal{R} = \mathcal{R}[\dot{\rho}, \dot{\mathbf{w}}]$ (for example, Joule heating) will not break the charge conservation law, as it gives rise to $\dot{\rho} = -q\boldsymbol{\nabla} \cdot (\delta_{\mathbf{w}}\mathcal{F} + \delta_{\dot{\mathbf{w}}}\mathcal{R})/\hbar$.

3. $\mathcal{Q}$-nonconserving dissipation

If we want to include dissipation that breaks the conservation law of Casimir invariants $\mathcal{Q}$, we have to use the more general version of the equations of motion given by [52]

$$\dot{X}_i(\mathbf{r}, t) = \int \mathrm{d}V' J_{ij}(\mathbf{r}, \mathbf{r}') f_j(\mathbf{r}', t) - \frac{\delta\mathcal{R}[\mathbf{f}]}{\delta f_i(\mathbf{r}, t)}. \quad \text{(D8)}$$

Here, the Rayleighian $\mathcal{R}[\mathbf{f}]$ is constructed as a functional of the forces $\mathbf{f} = \delta_{\mathbf{X}}\mathcal{F}$ thermodynamically conjugate to $\mathbf{X}$,

$$\mathcal{R}[\mathbf{f}] = \int \mathrm{d}V \int \mathrm{d}V' \frac{1}{2} f_i(\mathbf{r}, t) L_{ij}(\mathbf{r}, \mathbf{r}') f_j(\mathbf{r}', t), \quad \text{(D9)}$$

where $L_{ij}(\mathbf{r}, \mathbf{r}') = L_{ji}(\mathbf{r}', \mathbf{r})$ are dissipation coefficients. Crucially, this force construction $\mathcal{R}[\mathbf{f}]$ is not equivalent to the velocity construction $\mathcal{R}[\dot{\mathbf{X}}]$. Namely, as discussed above, whenever Casimir invariants $\mathcal{Q}$ are present, the Poisson operator $J_{ij}(\mathbf{r}, \mathbf{r}')$ is not invertible in Eq. (D1) to write the forces $\mathbf{f}$ as a functional of the velocities $\dot{\mathbf{X}}$. However, it is always possible to express velocities $\dot{\mathbf{X}}$ in terms of forces $\mathbf{f}$. Hence, when the functional depends implicitly on the forces through velocities, $\mathcal{R}[\mathbf{f}] = \mathcal{R}[\dot{\mathbf{X}}(\mathbf{f})]$, we can use the chain rule,

$$\begin{aligned} -\frac{\delta\mathcal{R}[\dot{\mathbf{X}}(\mathbf{f})]}{\delta f_i(\mathbf{r}, t)} &= -\int \mathrm{d}V' \frac{\delta\dot{X}_j(\mathbf{r}', t)}{\delta f_i(\mathbf{r}, t)} \frac{\delta\mathcal{R}[\dot{\mathbf{X}}]}{\delta\dot{X}_j(\mathbf{r}', t)} \\ &\approx -\int \mathrm{d}V' J_{ji}(\mathbf{r}', \mathbf{r}) \frac{\delta\mathcal{R}[\dot{\mathbf{X}}]}{\delta\dot{X}_j(\mathbf{r}', t)} \\ &= \int \mathrm{d}V' J_{ij}(\mathbf{r}, \mathbf{r}') \frac{\delta\mathcal{R}[\dot{\mathbf{X}}]}{\delta\dot{X}_j(\mathbf{r}', t)}, \end{aligned} \quad \text{(D10)}$$

and retrieve the $\mathcal{Q}$-conserving dissipation of Eq. (D6). In the second step, we have reinserted the equations of motion and, for simplicity, neglected higher orders in dissipation. In the third step, we use the antisymmetry of the Poisson operator, $J_{ji}(\mathbf{r}', \mathbf{r}) = -J_{ij}(\mathbf{r}, \mathbf{r}')$.

For our example of a magnet, it is easy to construct a Rayleighian from thermodynamic forces that breaks the local conservation law of $\mathcal{Q} = \mathbf{s}^2$. For example, using $\mathcal{R} = \int \mathrm{d}V\,\eta_{\mathbf{s}}\,\mathbf{f}_{\mathbf{s}}{}^2/2$ with dissipation coefficient $\eta_{\mathbf{s}}$, the equations of motion would be $\dot{\mathbf{s}} = -\mathbf{s} \times \mathbf{f}_{\mathbf{s}}/s - \eta_{\mathbf{s}}\mathbf{f}_{\mathbf{s}}$. Here, $\mathbf{f}_{\mathbf{s}}$ can have components along $\mathbf{s}$, so $\mathcal{Q}$ is allowed to change. We retrieve Landau-Lifshitz damping (which conserves $\mathcal{Q}$) by using $\mathcal{R} = \int \mathrm{d}V\,\eta_{\mathbf{s}}(\mathbf{s} \times \mathbf{f}_{\mathbf{s}})^2/2$, where we project out the components of $\mathbf{f}_{\mathbf{s}}$ parallel to $\mathbf{s}$.

Similarly, for our example of a superconductor, if we used a Rayleighian constructed from the thermodynamic forces, $\mathcal{R} = \int \mathrm{d}V\,\eta_\rho\, f_\rho^2/2$ with dissipation coefficient η_ρ, a violation of charge conservation would be possible, $\dot{\rho} = -q\boldsymbol{\nabla} \cdot \mathbf{f}_{\mathbf{w}}/\hbar - \eta_\rho f_\rho$.

4. Onsager symmetry

When constructing the Rayleighian, we have to respect the second law of thermodynamics and microscopic reversibility. The former prescribes that L_{ij} and R_{ij} must be positive-semidefinite matrices. The latter is manifest as Onsager reciprocity [65], which relates the coefficients via

$$L_{ij}(\mathbf{r}, \mathbf{r}') = \epsilon_j\epsilon_i\mathcal{T}[L]_{ji}(\mathbf{r}', \mathbf{r}), \quad \text{(D11)}$$

where $\mathcal{T}$ is the time-reversal operation. Thus, $\mathcal{T}[L]_{ji}$ transforms all (external and internal) fields that might be included in L_{ji}. In addition, $\mathcal{T}[X_i] = \varepsilon_i X_i$ defines the parity $\varepsilon_i = \pm 1$ under time reversal. Note that this relation ensures that the Rayleighian is even under time reversal,

$$\begin{aligned} \mathcal{T}[\mathcal{R}[\mathbf{f}]] &= \int \mathrm{d}V \int \mathrm{d}V' \frac{1}{2} f_j(\mathbf{r}', t)\epsilon_j\epsilon_i\mathcal{T}[L]_{ji}(\mathbf{r}', \mathbf{r}) f_i(\mathbf{r}, t) \\ &= \mathcal{R}[\mathbf{f}], \end{aligned} \quad \text{(D12)}$$

where we used that $\mathcal{T}[f_i] = \varepsilon_i f_i$ since $f_i = \delta_{X_i}\mathcal{F}$ and $\mathcal{T}[\mathcal{F}] = \mathcal{F}$. Hence, a Rayleighian that is Onsager symmetric has to be even under time reversal. An analog statement holds for the Rayleighian as a functional of velocities, $\mathcal{T}[\mathcal{R}[\dot{\mathbf{X}}]] = \mathcal{R}[\dot{\mathbf{X}}]$, where R_{ij} also fulfills the Onsager relations (as does the Poisson operator J_{ij}).

APPENDIX E: POISSON BRACKETS

Here, we microscopically motivate the Poisson brackets of the $\mathbf{d}$ vector and discuss the resulting Poisson brackets of the

hydrodynamic variables $\{\rho, \mathbf{s}, \mathbf{w}\}$ in 3D, while the 1D and 2D cases are implicit.

1. Microscopic motivation

To microscopically construct the $\mathbf{d}$-vector order parameter, we first require a pairing mechanism of electrons that is in accordance with the Pauli principle. To this end, we assume for each electron, in addition to a spatial and spin $\sigma \in \{\uparrow, \downarrow\}$ degree of freedom, an additional pseudospin $\tau \in \{+, -\}$. Then, we can realize, in principle, an electron pairing that is even in orbital space (s-wave), even in spin space (spin-triplet), and odd in pseudospin space (singlet), making it overall antisymmetric.

For example, in graphene-based systems, electrons are endowed with an additional valley degree of freedom, τ (where $\{+, -\}$ would correspond to inequivalent Dirac points $\{\mathbf{K}, \mathbf{K}'\}$), which is utilized in the field of valleytronics [66,67]. Then, as pointed out in Ref. [24], the spin-triplet order parameter $\mathcal{M} = \mathrm{SO}(3)$ can potentially be realized in bilayer graphene as an s-wave, spin-triplet, valley-singlet superconductor [13–15].

We write the ground state $|\Omega\rangle$ of the spin-triplet superconductor as a coherent state via [68]

$$|\Omega\rangle = \frac{1}{\sqrt{\mathcal{N}}} \exp\left[\int \mathrm{d}\mathbf{r}\, \mathbf{d}\cdot\boldsymbol{\Psi}^\dagger(\mathbf{r})\right]|0\rangle, \tag{E1}$$

where we assume a full spin polarization and a homogeneous order parameter $\mathbf{d}$. The modulus of the order parameter is $|\mathbf{d}| = d$ and $\mathbf{d}\cdot\mathbf{d} = 0$; see Eq. (A1). Here, $\boldsymbol{\Psi}^\dagger$ is the spin-triplet Cooper-pair creation operator and $|0\rangle$ is the bare electron vacuum state. The annihilation operator is defined as

$$\boldsymbol{\Psi}(\mathbf{r}) = \frac{1}{2\sqrt{2}d}(i\sigma_y\boldsymbol{\sigma})_{\sigma'\sigma}(i\tau_y)_{\tau'\tau}\int \mathrm{d}\mathfrak{r} f(\mathfrak{r})\psi_{\sigma,\tau}(\mathbf{r}+\mathfrak{r}/2) \times \psi_{\sigma',\tau'}(\mathbf{r}-\mathfrak{r}/2), \tag{E2}$$

where $\mathfrak{r}$ is the relative position of the two electrons and $\mathbf{r}$ is the center-of-mass position of the Cooper pair. The annihilation operator $\boldsymbol{\Psi}(\mathbf{r})$ is constructed out of two electron field operators with spin-triplet and pseudospin-singlet pairing encoded by $i\sigma_y\boldsymbol{\sigma}$ and $i\tau_y$, respectively. The spatial distribution of the Cooper pair is described by $f(\mathfrak{r})$, which decays over the coherence length ξ. The normalization constant in Eq. (E1) ensuring $\langle\Omega|\Omega\rangle = 1$ is given by $\mathcal{N} = \prod_{\mathbf{k}}(1+|f_{\mathbf{k}}|^2)$ with $f_{\mathbf{k}} = \int \mathrm{d}\mathfrak{r}\, e^{-i\mathbf{k}\cdot\mathfrak{r}} f(\mathfrak{r})$, where we assume inversion symmetry $f_{\mathbf{k}} = f_{-\mathbf{k}}$ [69].

Making a choice to normalize the $\mathbf{d}$-vector such that $d^2 = V^{-1}\sum_{\mathbf{k}}|f_{\mathbf{k}}|^2/(1+|f_{\mathbf{k}}|)^2$, in the coherent state, the expectation value of such a Cooper-pair operator is given by

$$\langle\boldsymbol{\Psi}(\mathbf{r})\rangle = \mathbf{d}. \tag{E3}$$

To perform the calculation, we used the relation $\mathrm{Tr}(\sigma_y\sigma_i\sigma_y^*\sigma_j^*) = 2\delta_{ij}$. By comparing with the mean electron number, we find

$$\sum_{\sigma,\tau}\langle\psi^\dagger_{\sigma,\tau}(\mathbf{r})\psi_{\sigma,\tau}(\mathbf{r})\rangle = \frac{2}{V}\sum_{\mathbf{k}}\frac{|f_{\mathbf{k}}|^2}{1+|f_{\mathbf{k}}|^2} = 2d^2. \tag{E4}$$

Hence, we can interpret $\mathbf{d}^*\cdot\mathbf{d} = d^2$ as the "Cooper-pair density," so that qd^2 with $q = -2e$ is the total charge density. Furthermore, we can identify the spin density via

$$\sum_{\sigma\sigma',\tau}\frac{\hbar}{2}\langle\psi^\dagger_{\sigma,\tau}(\mathbf{r})\boldsymbol{\sigma}_{\sigma\sigma'}\psi_{\sigma',\tau}(\mathbf{r})\rangle = i\hbar\mathbf{d}\times\mathbf{d}^* = \hbar d^2\mathbf{s}, \tag{E5}$$

which justifies the definition of spin orientation $\mathbf{s}$ in Eq. (A2) and makes $s = \hbar d^2$ the spin density of the system.

The analogy to bosonic degrees of freedom works well whenever the Cooper-pair operator $\boldsymbol{\Psi}(\mathbf{r})$ fulfills approximately bosonic commutation relations. Performing the calculation, we find

$$[\Psi_i(\mathbf{r}), \Psi_j(\mathbf{r}')] = 0. \tag{E6}$$

However, $[\Psi_i(\mathbf{r}), \Psi_j^\dagger(\mathbf{r}')] \neq \delta_{ij}\delta(\mathbf{r}-\mathbf{r}')$, which is expected as the electrons of a Cooper pair still adhere to the Pauli exclusion principle [70]. Our strategy is to perform an average of the commutator in the state $|\Omega\rangle$ to obtain

$$\langle[\Psi_i(\mathbf{r}), \Psi_j^\dagger(\mathbf{r}')]\rangle = \frac{\delta_{ij}}{V^2d^2}\sum_{\mathbf{k},\mathbf{k}'}e^{i(\mathbf{k}+\mathbf{k}')\cdot(\mathbf{r}-\mathbf{r}')}\frac{\left|f_{\frac{\mathbf{k}-\mathbf{k}'}{2}}\right|^2}{1+|f_{\mathbf{k}}|^2} = \delta_{ij}\tilde{\delta}(\mathbf{r}-\mathbf{r}'). \tag{E7}$$

Here, we identified the function $\tilde{\delta}(\mathbf{r})$, which is centered around $\mathbf{r} = 0$, has characteristic width of the coherence length ξ, and is normalized via $\int \mathrm{d}\mathbf{r}\tilde{\delta}(\mathbf{r}) = 1$. In the limit of vanishing coherence length, we get $\lim_{\xi\to 0}\tilde{\delta}(\mathbf{r}) = \delta(\mathbf{r})$.

Now, we can assume an order parameter $\mathbf{d}(\mathbf{r})$ that spatially varies on a coarse-grained scale ξ, such that $\tilde{\delta}(\mathbf{r}) \to \delta(\mathbf{r})$, and use the classical to quantum correspondence $[\cdot,\cdot] \to i\hbar\{\cdot,\cdot\}$ to obtain the desired Poisson brackets,

$$\{d_i(\mathbf{r}), d_j(\mathbf{r}')\} = 0, \tag{E8a}$$

$$\{d_i^*(\mathbf{r}), d_j(\mathbf{r}')\} = i\delta_{ij}\delta(\mathbf{r}-\mathbf{r}')/\hbar. \tag{E8b}$$

While the above derivations were performed for zero temperature, we expect that upon generalization to finite temperatures [71], the key qualitative results of Eqs. (E3)–(E8) will be retained.

2. Phenomenological foundation

The Poisson brackets between $\{\rho, \mathbf{s}, \mathbf{w}\}$ follow from Eqs. (A2) and (A3). After some straightforward algebra, we find

$$\{s_i(\mathbf{r}), s_j(\mathbf{r}')\} = \epsilon_{ijk}s_k\delta(\mathbf{r}-\mathbf{r}')/s, \tag{E9a}$$

$$\{w_i(\mathbf{r}), \rho(\mathbf{r}')\} = -q\partial_i\delta(\mathbf{r}-\mathbf{r}')/\hbar, \tag{E9b}$$

$$\{w_i(\mathbf{r}), w_j(\mathbf{r}')\} = q\epsilon_{ijk}(\nabla\times\mathbf{w})_k\delta(\mathbf{r}-\mathbf{r}')/\hbar\rho, \tag{E9c}$$

$$\{w_i(\mathbf{r}), \mathbf{s}(\mathbf{r}')\} = q\partial_i\mathbf{s}\,\delta(\mathbf{r}-\mathbf{r}')/\hbar\rho, \tag{E9d}$$

which are derived for zero temperature, where the spin density is $s = \hbar d^2$ and the charge density is $\rho = qd^2$. Note that Eqs. (E9a) and (E9b) are fundamental. The former identifies s_i as generators of spin rotations and the latter identifies charge density as the generator of U(1) phase rotations. Furthermore, Eq. (E9c) encodes the Magnus force on superconducting vortices and Eq. (E9d) captures spin advection by the superflow and, thereby, the adiabatic spin-transfer torque and its Onsager reciprocal motive force [72].

Due to the above physical arguments, we expect these Poisson brackets to qualitatively hold also for finite temperatures, where s and ρ are promoted to total spin and charge densities, respectively, including both normal and superconducting contributions. However, depending on details, there might be slight modifications to the Poisson brackets. For example, allowed modifications on the right-hand side of Eqs. (E9) are given by $\rho \to \rho - C$ and $s \to P\hbar(\rho - C)/q$, where P describes the spin polarization and C captures effects from quasiparticles [73]. These modifications still guarantee the Jacobi identity,

$$\{X_i(\mathbf{r}), \{X_j(\mathbf{r}'), X_k(\mathbf{r}'')\}\} + \{X_j(\mathbf{r}'), \{X_k(\mathbf{r}''), X_i(\mathbf{r})\}\} + \{X_k(\mathbf{r}''), \{X_i(\mathbf{r}), X_j(\mathbf{r}')\}\} = 0, \tag{E10}$$

allowing for a consistent Hamiltonian theory. Besides the Jacobi identity, we also require that for a theory with an SO(3) order parameter, the Mermin-Ho relation [see Eq. (A5)] is dynamically maintained at all times. This necessitates $P = 1$, as deviations of P from this value would violate Eq. (F18) below.

Our phenomenology can be qualitatively extended to systems where superfluid winding $\mathbf{w}$ coexists with a local angular momentum $\mathbf{s}$, such that the degrees of freedom are still given by $\{\rho, \mathbf{s}, \mathbf{w}\}$. For such systems, the Mermin-Ho relation as presented in Eq. (A5) can be relaxed. However, topology would still dictate that the change in phase winding around a loop upon passage of a full skyrmion through the loop is given by $\delta\mathcal{W} = 2\pi n$ with $n \in \mathbb{Z}$. Under such a constraint, the polarization P can only take on half-integer values, $P \in \mathbb{Z}/2$, and the Mermin-Ho relation is modified to be $(\nabla \times \mathbf{w})_k = P\epsilon_{ijk}\mathbf{s} \cdot (\partial_i \mathbf{s} \times \partial_j \mathbf{s})/2$. If P does not take on these values, it would be an indication that the theory is incomplete and more degrees of freedom beyond $\{\rho, \mathbf{s}, \mathbf{w}\}$ need to be introduced to self-consistently capture the dynamics of the system.

APPENDIX F: EQUATIONS OF MOTION

In this appendix, we derive the equations of motion for a 3D triplet superconductor, which can be written in terms of the fields $\mathbf{X} = \{\rho, \mathbf{s}, \mathbf{w}, \mathbf{A}, \mathbf{E}\}$, with the total charge density ρ (per unit volume), the spin orientation field $\mathbf{s}$, the superconducting winding density $\mathbf{w}$, the magnetic vector potential $\mathbf{A}$, and the electric field $\mathbf{E}$. Here, we have assumed the Weyl gauge [74]. Once the Poisson brackets, the free energy $\mathcal{F}$, and the Rayleighian $\mathcal{R}$ are specified, we can use Eq. (D6) to derive the equations of motion.

The Poisson brackets between $\{\rho, \mathbf{s}, \mathbf{w}\}$ are given by Eq. (E9), which (after taking the Weyl gauge) have to be supplemented by the canonical Poisson bracket between $\mathbf{A}$ and $\mathbf{E}$,

$$\{E_i(\mathbf{r}), A_j(\mathbf{r}')\} = 4\pi c\, \delta_{ij}\delta(\mathbf{r} - \mathbf{r}'), \tag{F1}$$

to capture the electrodynamics. The remaining Poisson brackets vanish.

The free energy can be phenomenologically constructed as

$$\mathcal{F}[\rho, \mathbf{s}, \mathbf{w}, \mathbf{A}, \mathbf{E}] = \int \mathrm{d}V \left[\frac{A}{2}(\nabla \mathbf{s})^2 - \gamma s \mathbf{s} \cdot \mathbf{B} + \frac{1}{2\chi_w}\left(\mathbf{w} - \frac{q}{\hbar c}\mathbf{A}\right)^2 + \frac{(\rho - \rho_0)^2}{2\chi_c} + \frac{\mathbf{B}^2 + \mathbf{E}^2}{8\pi}\right], \tag{F2}$$

which has been written using the magnetic field $\mathbf{B} = \nabla \times \mathbf{A}$. Here, A is the spin stiffness, χ_w is the winding compressibility, χ_c is the charge compressibility, and $\gamma < 0$ is the gyromagnetic ratio. The connection between the free energy in Eq. (F2) and the Ginzburg-Landau free energy for the order parameter $\mathbf{d}$ is elucidated via

$$\frac{A_d}{2}\left|\left(\nabla - i\frac{q}{\hbar c}\mathbf{A}\right)\mathbf{d}\right|^2 = \frac{A_d\rho}{4}(\nabla \mathbf{s})^2 + \frac{A_d\rho}{2}\left(\mathbf{w} - \frac{q}{\hbar c}\mathbf{A}\right)^2 + \frac{A_d\rho}{2}(\nabla\sqrt{\rho})^2. \tag{F3}$$

We find that this produces three terms which, respectively, are analogous to the spin exchange energy, the superconducting winding energy, and a term also referred to as "quantum pressure" [75] that is neglected in our analysis. Generically, we may expect that the prefactors of each of these terms are independent phenomenological parameters, rather than being related via A_d. This results in the spin exchange coefficient A and the effective winding compressibility χ_w.

Energy dissipation is governed by the Rayleigh functional $\mathcal{R}$, which is bilinear in the velocities $\dot{\mathbf{X}}$,

$$\mathcal{R} = \int \mathrm{d}V \left\{\frac{\alpha s}{2}(\partial_t \mathbf{s})^2 + \frac{\sigma}{2}\left[\frac{\hbar}{q}\partial_t\left(\mathbf{w} - \frac{q\mathbf{A}}{\hbar c}\right)\right]^2\right\}. \tag{F4}$$

The first term corresponds to Gilbert damping with damping coefficient α and the second term describes Joule heating with conductivity σ. Now, we have all the ingredients to derive the equations of motion.

1. Charge continuity

For the charge density ρ, there is one nonzero Poisson bracket,

$$\begin{aligned}
&\int \mathrm{d}V' \{\rho(\mathbf{r}), w_j(\mathbf{r}')\}\left[\frac{\delta\mathcal{F}}{\delta w_j(\mathbf{r}')} + \frac{\delta\mathcal{R}}{\delta\dot{X}_j(\mathbf{r}')}\right] \\
&= \int \mathrm{d}V' [\partial'_j\delta(\mathbf{r}' - \mathbf{r})]\left\{\frac{q}{\hbar\chi_w}\left[w_j(\mathbf{r}') - \frac{q}{\hbar c}A_j(\mathbf{r}')\right] + \frac{\hbar\sigma}{q}\left[\dot{w}_j(\mathbf{r}') - \frac{q}{\hbar c}\dot{A}_j(\mathbf{r}')\right]\right\} \\
&= -\nabla \cdot \left[\frac{q}{\hbar\chi_w}\left(\mathbf{w} - \frac{q\mathbf{A}}{\hbar c}\right) + \frac{\hbar\sigma}{q}\left(\dot{\mathbf{w}} - \frac{q\dot{\mathbf{A}}}{\hbar c}\right)\right] \\
&= -\nabla \cdot (\mathbf{j} + \sigma\boldsymbol{\mathcal{E}}),
\end{aligned} \tag{F5}$$

where, in the last step, we identified the supercurrent $\mathbf{j} = \frac{q}{\hbar\chi_w}(\mathbf{w} - \frac{q\mathbf{A}}{\hbar c})$ and the normal current $\sigma\boldsymbol{\mathcal{E}}$ stemming from the total electromotive force, $\boldsymbol{\mathcal{E}} = \mathbf{E} + \hbar\dot{\mathbf{w}}/q$. The equation of motion becomes

$$\boxed{\partial_t \rho = -\nabla \cdot \mathfrak{J}}, \tag{F6}$$

where the total current is $\mathfrak{J} = \mathbf{j} + \sigma\boldsymbol{\mathcal{E}}$.

2. Landau-Lifshitz-Gilbert equation

For the spin orientation $\mathbf{s}$, we have two nonzero Poisson brackets. The first Poisson bracket generates the precession and Gilbert damping term,

$$\begin{aligned}&\int \mathrm{d}V'\,\{s_i(\mathbf{r}), s_j(\mathbf{r}')\}\left[\frac{\delta\mathcal{F}}{\delta s_j(\mathbf{r}')}+\frac{\delta\mathcal{R}}{\delta\dot{s}_j(\mathbf{r}')}\right]\\&=\int \mathrm{d}V'\,\epsilon_{ijk}s_k(\mathbf{r})\delta(\mathbf{r}-\mathbf{r}')\left[\frac{1}{s(\mathbf{r}')}\frac{\delta\mathcal{F}}{\delta s_j(\mathbf{r}')}+\alpha\dot{s}_j(\mathbf{r}')\right]\\&=\epsilon_{ijk}s_j(\mathbf{H}_{\mathrm{eff}}-\alpha\dot{\mathbf{s}})_k,\end{aligned}\tag{F7}$$

where we defined the effective field,

$$\mathbf{H}_{\mathrm{eff}}\equiv-\frac{1}{s}\frac{\delta\mathcal{F}}{\delta\mathbf{s}}=\frac{A}{s}\nabla^2\mathbf{s}+\gamma\mathbf{B}.\tag{F8}$$

The second Poisson bracket generates the spin-transfer torque,

$$\begin{aligned}&\int \mathrm{d}V'\,\{s_i(\mathbf{r}), w_j(\mathbf{r}')\}\left[\frac{\delta\mathcal{F}}{\delta w_j(\mathbf{r}')}+\frac{\delta\mathcal{R}}{\delta\dot{w}_j(\mathbf{r}')}\right]\\&=-\int \mathrm{d}V'\frac{1}{\rho}[\partial'_j s_i(\mathbf{r}')]\delta(\mathbf{r}-\mathbf{r}')\mathfrak{J}_j(\mathbf{r}')\\&=-\frac{\mathfrak{J}}{\rho}\cdot\nabla s_i,\end{aligned}\tag{F9}$$

where we have identified the total current $\mathfrak{J}$. Hence, the Landau-Lifshitz-Gilbert equation is given by

$$\boxed{\partial_t\mathbf{s}=\mathbf{s}\times\mathbf{H}_{\mathrm{eff}}-\alpha\mathbf{s}\times\partial_t\mathbf{s}-\frac{\mathfrak{J}}{\rho}\cdot\nabla\mathbf{s}}.\tag{F10}$$

3. Winding continuity equation

For the winding density $\mathbf{w}$, we have three nonzero Poisson brackets. The first Poisson bracket generates a Magnus term,

$$\begin{aligned}&\int \mathrm{d}V'\,\{w_i(\mathbf{r}), w_j(\mathbf{r}')\}\left[\frac{\delta\mathcal{F}}{\delta w_j(\mathbf{r}')}+\frac{\delta\mathcal{R}}{\delta\dot{w}_j(\mathbf{r}')}\right]\\&=\int \mathrm{d}V'\,\frac{1}{\rho}\epsilon_{ijk}[\nabla\times\mathbf{w}(\mathbf{r})]_k\delta(\mathbf{r}-\mathbf{r}')\mathfrak{J}_j(\mathbf{r}')\\&=\frac{1}{\rho}\epsilon_{ijk}\mathfrak{J}_j(\nabla\times\mathbf{w})_k.\end{aligned}\tag{F11}$$

The second Poisson bracket generates the term

$$\begin{aligned}&\int \mathrm{d}V'\,\{w_i(\mathbf{r}), s_j(\mathbf{r}')\}\left[\frac{\delta\mathcal{F}}{\delta s_j(\mathbf{r}')}+\frac{\delta\mathcal{R}}{\delta\dot{s}_j(\mathbf{r}')}\right]\\&=-\int \mathrm{d}V'\,[\partial_i s_j(\mathbf{r})]\delta(\mathbf{r}-\mathbf{r}')[\mathbf{H}_{\mathrm{eff}}(\mathbf{r}')-\alpha\dot{\mathbf{s}}(\mathbf{r}')]_j\\&=-(\partial_i s_j)(\mathbf{H}_{\mathrm{eff}}-\alpha\dot{\mathbf{s}})_j,\end{aligned}\tag{F12}$$

where we have assumed full polarization, $s=\hbar\rho/q$, in accordance with the zero-temperature limit $\rho=qd^2$ and $s=\hbar d^2$. Finally, the third Poisson bracket generates the term

$$\begin{aligned}&\int \mathrm{d}V'\,\{w_i(\mathbf{r}), \rho(\mathbf{r}')\}\left[\frac{\delta\mathcal{F}}{\delta\rho(\mathbf{r}')}+\frac{\delta\mathcal{R}}{\delta\dot{\rho}(\mathbf{r}')}\right]\\&=\int \mathrm{d}V'\,\frac{q}{\hbar}[\partial'_i\delta(\mathbf{r}-\mathbf{r}')]\mu(\mathbf{r}')\\&=-\frac{q}{\hbar}\partial_i\mu,\end{aligned}\tag{F13}$$

where we have defined the chemical potential,

$$\mu=\frac{\delta\mathcal{F}}{\delta\rho}=\frac{\rho-\rho_0}{\chi_c}-\frac{\gamma\hbar}{q}\mathbf{s}\cdot\mathbf{B}.\tag{F14}$$

Putting it all together, the equation becomes

$$\begin{aligned}\partial_t\mathbf{w}=&-\frac{q}{\hbar}\nabla\mu+\frac{\mathfrak{J}}{\rho}\times(\nabla\times\mathbf{w})\\&-\{\mathbf{s}\times[(\mathbf{H}_{\mathrm{eff}}-\alpha\dot{\mathbf{s}})\times\mathbf{s}]\}\cdot\nabla\mathbf{s},\end{aligned}\tag{F15}$$

where, for the last term, we have used that $\nabla\mathbf{s}$ is orthogonal to $\mathbf{s}$, allowing us to introduce the projection $\mathbf{s}\times(\ldots\times\mathbf{s})$. Reinserting the Landau-Lifshitz-Gilbert equation from Eq. (F10), we get

$$\begin{aligned}\partial_t\mathbf{w}=&-\frac{q}{\hbar}\nabla\mu+\frac{\mathfrak{J}}{\rho}\times(\nabla\times\mathbf{w})\\&+\left[\mathbf{s}\times\left(\partial_t\mathbf{s}+\frac{\mathfrak{J}}{\rho}\cdot\nabla\mathbf{s}\right)\right]\cdot\nabla\mathbf{s}.\end{aligned}\tag{F16}$$

It is convenient to define the emergent electric field $e_i=\hbar\mathbf{s}\cdot(\partial_t\mathbf{s}\times\partial_i\mathbf{s})/q$ and the emergent magnetic field $b_i=-\hbar c\epsilon_{ijk}\mathbf{s}\cdot(\partial_j\mathbf{s}\times\partial_k\mathbf{s})/2q$ due to the spin texture, so that we can write

$$\partial_t\mathbf{w}=-\frac{q}{\hbar}\nabla\mu+\frac{\mathfrak{J}}{\rho}\times\left(\nabla\times\mathbf{w}+\frac{q}{\hbar c}\mathbf{b}\right)+\frac{q}{\hbar}\mathbf{e}.\tag{F17}$$

As a next step, we implement the Mermin-Ho relation from Eq. (A5), which can be rewritten as $\nabla\times\mathbf{w}=-\frac{q}{\hbar c}\mathbf{b}$. To see how this relation dynamically evolves, we apply the rotation to Eq. (F17) and obtain

$$\partial_t\left(\nabla\times\mathbf{w}+\frac{q}{\hbar c}\mathbf{b}\right)=\nabla\times\left[\frac{\mathfrak{J}}{\rho}\times\left(\nabla\times\mathbf{w}+\frac{q}{\hbar c}\mathbf{b}\right)\right],\tag{F18}$$

where we used that $\nabla\times\mathbf{e}=-\partial_t\mathbf{b}/c$ for $|\mathbf{s}|=1$. Hence, by choosing an initial configuration of $\mathbf{w}$ and $\mathbf{s}$ that fulfills the Mermin-Ho relation, the equations of motion guarantee that the Mermin-Ho relation is fulfilled for all later times. Then, we obtain the simple equation

$$\boxed{\partial_t\mathbf{w}=\frac{q}{\hbar}(-\nabla\mu+\mathbf{e})}.\tag{F19}$$

Note that the equation of motion can be rewritten as a spin-triplet version of the first Josephson relation,

$$\partial_t \mathbf{j} = \frac{q^2}{\hbar^2 \chi_w} \boldsymbol{\mathcal{E}}, \tag{F20}$$

where the electromotive force is $\boldsymbol{\mathcal{E}} = \mathbf{E} - \nabla\mu + \mathbf{e}$. Similarly, the spin-triplet version of the second Josephson relation becomes, with Eq. (A5),

$$\nabla \times \mathbf{j} = -\frac{q^2}{\hbar^2 \chi_w c} \boldsymbol{\mathcal{B}}, \tag{F21}$$

where the total effective magnetic field is given by $\boldsymbol{\mathcal{B}} = \mathbf{B} + \mathbf{b}$.

4. Ampère's law

For the electric field $\mathbf{E}$, there is only one nonzero Poisson bracket,

$$\begin{aligned}
&\int \mathrm{d}V' \{E_i(\mathbf{r}), A_j(\mathbf{r}')\}\left[\frac{\delta \mathcal{F}}{\delta A_j(\mathbf{r}')} + \frac{\delta \mathcal{R}}{\delta \dot{A}_j(\mathbf{r}')}\right] \\
&= -\int \mathrm{d}V' 4\pi \delta_{ij} \delta(\mathbf{r} - \mathbf{r}') \Big\{ \mathfrak{J}_j(\mathbf{r}') + c\epsilon_{jkl} \partial'_k [M_l(\mathbf{r}')] \\
&\quad - \frac{c}{4\pi} \epsilon_{jkl} \partial'_k [\epsilon_{lmn} \partial'_m A_n(\mathbf{r}')] \Big\} \\
&= (-4\pi \boldsymbol{\mathfrak{J}} - 4\pi c \nabla \times \mathbf{M} + c \nabla \times \mathbf{B})_i,
\end{aligned} \tag{F22}$$

where we defined the magnetization $\mathbf{M} = \gamma s \mathbf{s}$. Hence, the equation becomes

$$\boxed{\partial_t \mathbf{E} = -4\pi \boldsymbol{\mathfrak{J}} + c \nabla \times (\mathbf{B} - 4\pi \mathbf{M})}. \tag{F23}$$

This confirms that $\boldsymbol{\mathfrak{J}}$ is the total charge current in the system. Furthermore, the equation for $\mathbf{A}$ just reproduces the Weyl gauge, $\partial_t \mathbf{A} = -c\mathbf{E}$. While $\nabla \cdot \mathbf{B} = 0$ is automatically fulfilled, Gauss's law $\nabla \cdot \mathbf{E} = 4\pi\rho$ has to be imposed as an additional constraint. Finally, we can calculate the London penetration depth λ for a homogeneous spin texture $\mathbf{s}$, by applying the rotation to Eq. (F23) and inserting Eq. (F21). We obtain

$$\nabla^2 \mathbf{B} = -\frac{4\pi q^2}{\hbar^2 \chi_w c^2} \mathbf{B}, \tag{F24}$$

where we assumed $\partial_t \mathbf{E} = 0$ as well as zero dissipation. This allows the identification $\lambda = (\hbar c/q)\sqrt{\chi_w/4\pi}$.

APPENDIX G: TOPOLOGICAL HYDRODYNAMICS

Topological hydrodynamics of phase winding in 1D spin-triplet superconductors with static spin textures was discussed in the second-to-last paragraph of Sec. IV. In the following sections, we study the different flavors of topological hydrodynamics that arise in 2D and 3D spin-triplet superconductors.

1. Vorticity in 2D

For a 2D system, we can derive a topological continuity equation for superconducting vorticity,

$$\varrho_v = \mathbf{z} \cdot (\nabla \times \mathbf{w}). \tag{G1}$$

To this end, we write Eq. (F19) in 2D to obtain

$$\partial_t \mathbf{w} = -\frac{q}{\hbar} \nabla\mu - \mathbf{z} \times \mathbf{j}_{\mathrm{sk}}, \tag{G2}$$

where the skyrmion flux is given by $\mathbf{j}_{\mathrm{sk}} = \mathbf{s} \cdot [\partial_t \mathbf{s} \times (\mathbf{z} \times \nabla)\mathbf{s}]$. By applying the rotation to Eq. (G2), we immediately obtain the continuity equation for vorticity,

$$\partial_t \varrho_v = -\nabla \cdot \mathbf{j}_v, \tag{G3}$$

where we identified $\mathbf{j}_v = \mathbf{j}_{\mathrm{sk}}$. In fact, using the Mermin-Ho relation (A5) in 2D, we get $\varrho_v = \varrho_{\mathrm{sk}}$. Therefore, Eq. (G3) implies $\partial_t \varrho_{\mathrm{sk}} = -\nabla \cdot \mathbf{j}_{\mathrm{sk}}$, confirming that magnetic skyrmions take the role of superconducting coreless vortices in SO(3) spin-triplet superconductors. In fact, the skyrmion charge $\mathcal{Q} = \int \mathrm{d}A\, \varrho_{\mathrm{sk}}/4\pi$ is a global Casimir invariant; see Appendix D. The conservation is rooted in the relative homotopy $\pi_2[\mathrm{SO}(3), \mathrm{U}(1)] = \mathbb{Z}$, which makes them nonlocal objects; see Appendix B. This nonlocality also makes them energetically costly since an isolated skyrmion induces a supercurrent circulating around the skyrmion that falls off as $\sim 1/|\mathbf{r}|$. While the magnetic exchange energy is finite and given by the Belavin-Polyakov limit [76], the winding energy associated with the supercurrent diverges logarithmically as we integrate over the whole plane. In the main text, we circumvent this issue by considering a quasi-one-dimensional system, where the energy given by the magnetic exchange and the superconducting winding energy is finite.

2. Helicity in 3D

For a 3D system, we can derive a topological continuity equation for the superconducting helicity density,

$$\varrho_h = \mathbf{w} \cdot (\nabla \times \mathbf{w}), \tag{G4}$$

in analogy to fluid dynamics [77–79] and magnetohydrodynamics [80,81], where the winding $\mathbf{w}$ is replaced by the velocity field $\mathbf{v}$ in the former case and the magnetic vector potential $\mathbf{A}$ in the latter case. After some algebra, we find, from Eq. (F19),

$$\partial_t \varrho_h = -\nabla \cdot \left[\mathbf{w} \times \frac{q}{\hbar}(\nabla\mu + \mathbf{e})\right] - \frac{2q^2 \mathbf{e} \cdot \mathbf{b}}{\hbar^2 c}. \tag{G5}$$

We show that the source term $\mathbf{e} \cdot \mathbf{b}$ is identically zero by rewriting it as

$$\begin{aligned}
-\frac{2q^2 \mathbf{e} \cdot \mathbf{b}}{\hbar^2 c} &= \epsilon_{ijk} \mathbf{s} \cdot (\partial_t \mathbf{s} \times \partial_i \mathbf{s}) \mathbf{s} \cdot (\partial_j \mathbf{s} \times \partial_k \mathbf{s}) \\
&= \epsilon_{ijk} (\partial_t \mathbf{s} \times \partial_i \mathbf{s}) \cdot (\partial_j \mathbf{s} \times \partial_k \mathbf{s}) \\
&= 2\epsilon_{ijk} (\partial_t \mathbf{s} \cdot \partial_j \mathbf{s})(\partial_i \mathbf{s} \cdot \partial_k \mathbf{s}) = 0.
\end{aligned} \tag{G6}$$

In the second line, we have used the fact that $\partial_t \mathbf{s} \times \partial_i \mathbf{s} \propto \partial_j \mathbf{s} \times \partial_k \mathbf{s} \propto \mathbf{s}$, which follows from $|\mathbf{s}| = 1$. Finally, in the third line, we use that the contraction of the symmetric term $\partial_i \mathbf{s} \cdot \partial_j \mathbf{s}$ with the antisymmetric Levi-Civita symbol ϵ_{ijk} yields zero. Thus, we obtain the conservation law of helicity density in 3D,

$$\partial_t \varrho_h = -\nabla \cdot \mathbf{j}_h, \tag{G7}$$

where $\mathbf{j}_h = \mathbf{w} \times \frac{q}{\hbar}(\nabla\mu + \mathbf{e})$. Here, the integrated superconducting helicity density corresponds to a topological charge, $\mathcal{Q}_h = \int \mathrm{d}V\, \varrho_h/16\pi^2$, rooted in the bulk homotopy,

$\pi_3[\mathrm{SO}(3)] = \mathbb{Z}$, known as Shankar skyrmions [82] in the superfluid ^{3}He -A phase [83]. Making the projection $\mathrm{SO}(3) \to S^2$, wherein the triad $\{\mathbf{e}_1, \mathbf{e}_2, \mathbf{s}\}$ reduces to $\mathbf{s}$, the charge $\mathcal{Q}_h$ counts hopfions [84,85], which are topologically protected structures classified via $\pi_3(S^2) = \mathbb{Z}$. Finally, we remark that the term $\mathbf{e} \cdot \mathbf{b}$ can be nonzero if the magnitude of $\mathbf{s}$ is allowed to vary. Therefore, the presence of magnetic hedgehog dynamics [86] would spoil the conservation law since, at the core of the hedgehog, the magnitude of $\mathbf{s}$ goes to zero.

APPENDIX H: STABILITY ANALYSIS

In this appendix, we analyze the stability of the spin and superconducting winding texture of the 1D ring that occurs in the adiabatic operation of the spin-triplet SQUID. To this end, we rewrite the equations of motion from Eqs. (11a)–(11c) via

$$\partial_t \rho = -\partial_\ell (j + \sigma \mathcal{E}), \tag{H1a}$$

$$\partial_t \tilde{\mathbf{s}} = \frac{A}{s} \tilde{\mathbf{s}} \times D_\ell^2 \tilde{\mathbf{s}} - \alpha \tilde{\mathbf{s}} \times \partial_t \tilde{\mathbf{s}} - \frac{j + \sigma \mathcal{E}}{\rho} D_\ell \tilde{\mathbf{s}}, \tag{H1b}$$

$$\partial_t j = \frac{q^2}{\hbar^2 \chi_w} \mathcal{E}, \tag{H1c}$$

where we introduced the rotated spin texture $\tilde{\mathbf{s}}(\ell, t) = R(\ell)\mathbf{s}(\ell, t)$ defined such that the ground state becomes collinear, $\tilde{\mathbf{s}} = \mathbf{z}$. Here, s and ρ are the spin and charge density per unit length, respectively. For consistency, the partial derivative must be replaced by the covariant derivative $D_\ell \tilde{\mathbf{s}} = (\partial_\ell + R \partial_\ell R^{-1}) \tilde{\mathbf{s}}$. Next, we linearize these equations using

$$\begin{aligned} \rho(\ell, t) &\to \rho + \delta\rho(\ell, t), \\ \tilde{\mathbf{s}}(\ell, t) &\to \tilde{\mathbf{s}} + \delta\tilde{\mathbf{s}}(\ell, t), \\ j(\ell, t) &\to j + \delta j(\ell, t). \end{aligned} \tag{H2}$$

Here, our zeroth-order ansatz is given by a constant current j, a constant charge density ρ, and the spin texture $\tilde{\mathbf{s}} = \mathbf{z}$. After a Fourier transform of the fluctuations, $\delta\mathbf{X} = (\delta\tilde{s}_x, \delta\tilde{s}_y, \delta j, \delta\rho)$ (effectively replacing $\partial_t \delta\mathbf{X} \to -i\omega\delta\mathbf{X}$ and $\partial_\ell \delta\mathbf{X} \to ik\mathbf{X}$), we obtain the eigenvalue equation,

$$\omega\, \delta\mathbf{X}(k) = \Omega(k)\, \delta\mathbf{X}(k), \tag{H3}$$

for the eigenmodes with frequency ω. Here, the matrix Ω is a function of the wave number k, which, for the ring, only takes discrete values $k = 2\pi m/L$ with $m \in \mathbb{Z}$. In the following, we discuss separately fluctuations for the regimes with collinear and noncollinear spin texture.

1. Collinear spin texture

For the collinear spin texture, the ground state is $\mathbf{s} = \mathbf{z}$. Hence, no rotation is required, $R = \mathbb{I}$, in order to achieve $\tilde{\mathbf{s}} = \mathbf{s}$. For the fluctuations, we find

$$\Omega = \begin{pmatrix} -i\frac{\alpha A k^2}{s} + \frac{jk}{\rho} & i\frac{Ak^2}{s} + \frac{\alpha jk}{\rho} & 0 & 0 \\ -i\frac{Ak^2}{s} - \frac{\alpha jk}{\rho} & -i\frac{\alpha Ak^2}{s} + \frac{jk}{\rho} & 0 & 0 \\ 0 & 0 & 0 & \frac{kq^2}{\chi_c \chi_w \hbar^2} \\ 0 & 0 & k & -i\frac{k^2\sigma}{\chi_c} \end{pmatrix}. \tag{H4}$$

From this, we obtain for the spin waves the quadratic dispersion

$$\omega(k) = (Ak^2/s + jk/\rho)(1 - i\alpha), \tag{H5}$$

which is Doppler shifted by the supercurrent j due to the spin-transfer torque. For the charge and current degrees of freedom, we obtain the linear dispersion $\omega_q = kq/\hbar\sqrt{\chi_c \chi_w} - ik^2\sigma/\chi_c + \mathcal{O}(\sigma^2)$. Note the caveat that a full treatment of fluctuations in $\mathbf{E}$ and $\mathbf{B}$ would gap these modes (in accordance with the Higgs mechanism) to $\omega_q \to \sqrt{\omega_q^2 + \omega_p^2}$, where the plasma frequency is given by $\omega_p^2 = 4\pi q^2/\hbar^2 \chi_w$. Hence, in the following, we are only concerned with the low-energy spin-wave modes.

For stability, we have to ensure that $\mathrm{Im}\,\omega(k) < 0$. To satisfy this stability condition, we find that the current can only be increased up to

$$j = -A\frac{q}{\hbar}\frac{2\pi}{L} = -\kappa j_0 = -j^{\max} \tag{H6}$$

before the dispersion dips too low [see Fig. 5(a)], and the lowest-energy mode at $k = 2\pi/L$ becomes unstable. In the second step, we have used the definitions $j_0 = 2\pi q/\hbar\chi_w L$ and $\kappa = A\chi_w$ from the main text. Once the instability is reached, this initiates the nonsingular phase slip.

2. Noncollinear spin texture

During the nonsingular phase slip, the spin texture traces out a skyrmion and, therefore, becomes noncollinear. This conical spin texture is described by

$$\mathbf{s}(\ell) = \begin{pmatrix} \sin\theta\cos\varphi(\ell) \\ \sin\theta\sin\varphi(\ell) \\ \cos\theta \end{pmatrix}, \tag{H7}$$

where $\varphi(\ell) = p\ell$ and $p = 2\pi l/L$. To map the twisted texture $\mathbf{s}(\ell)$ to a collinear one, $\tilde{\mathbf{s}} = \mathbf{z}$, we introduce a position-dependent rotation matrix, $R(\ell) = R(\mathbf{y}, -\theta)R(\mathbf{z}, -\varphi)$. This gives rise to the covariant chiral derivative,

$$D_\ell \tilde{\mathbf{s}} = \left[\partial_\ell + p \begin{pmatrix} -\sin\theta \\ 0 \\ \cos\theta \end{pmatrix} \times \right] \tilde{\mathbf{s}}. \tag{H8}$$

In this case, the Landau-Lifshitz-Gilbert equation gives rise to a zeroth-order condition that the spin torque must be zero, which is ensured by

$$j = -A\frac{q}{\hbar} p \cos\theta. \tag{H9}$$

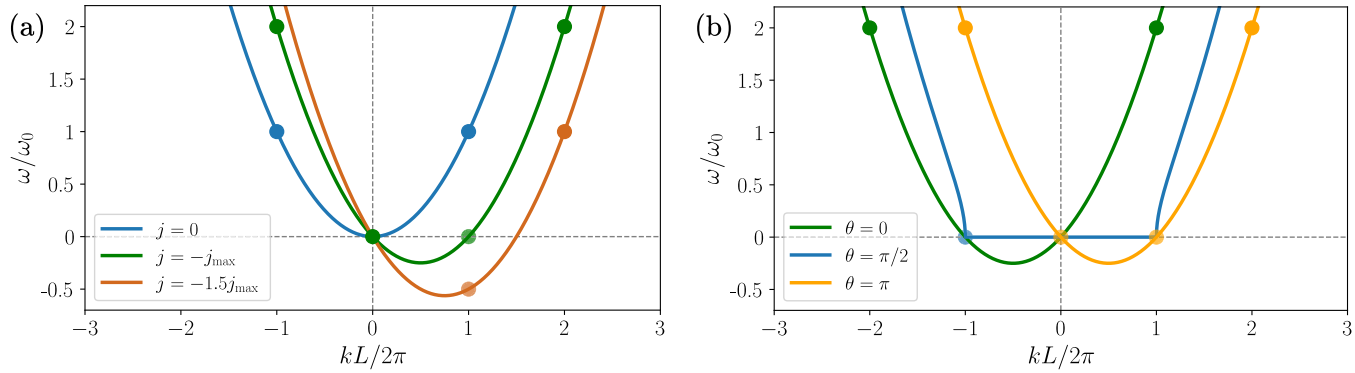

FIG. 5. Spin-wave excitation spectrum for (a) a collinear spin texture and (b) a noncollinear spin texture. In (a), once the current is lower than $j = -j^{\max}$, the mode at $k = 2\pi/L$ becomes unstable. In (b), the quadratic dispersion is shifted from left (green) to right (orange) as the phase slip is carried out. We defined $\omega_0 = A(2\pi)^2/L^2 s$.

Using this relation, we obtain, for the fluctuations,

$$\Omega = \begin{pmatrix} -i\frac{\alpha A\left(k^2-p^2\sin^2\theta\right)}{s} - \frac{jk}{\rho} & i\frac{Ak^2}{s} - \frac{\alpha jk}{\rho} & -i\frac{\alpha p\sin\theta}{\rho} & 0 \\ -i\frac{A\left(k^2-p^2\sin^2\theta\right)}{s} + \frac{\alpha jk}{\rho} + \frac{\sigma kp^2\hbar j\sin^2\theta}{q\rho^2} & -i\frac{\alpha Ak^2}{s} - \frac{jk}{\rho} - i\frac{\sigma Ak^2p^2\hbar\sin^2\theta}{qs\rho} & -i\frac{p\sin\theta}{\rho} & -\frac{kp\sigma\sin\theta}{\rho\chi_c} \\ \frac{pq\sin\theta}{\hbar\chi_w}\left[-i\frac{\alpha A\left(k^2-p^2\sin^2\theta\right)}{s} - \frac{jk}{\rho}\right] & \frac{pq\sin\theta}{\hbar\chi_w}\left[i\frac{Ak^2}{s} - \frac{\alpha jk}{\rho}\right] & -i\frac{\alpha p^2q\sin^2\theta}{\hbar\chi_w\rho} & \frac{kq^2}{\chi_c\chi_w\hbar^2} \\ i\frac{\sigma k^2p\hbar j\sin\theta}{q\rho} & \frac{\sigma Ak^3p\hbar\sin\theta}{qs} & k & -i\frac{k^2\sigma}{\chi_c} \end{pmatrix}. \tag{H10}$$

Here, we find, in the limit of zero dissipation $\sigma = \alpha = 0$ and vanishing charge compressibility $\chi_c \to 0$, the dispersion

$$\omega(k) = \frac{A}{s}\left(pk\cos\theta + \sqrt{k^4 - p^2k^2\sin^2\theta}\right). \tag{H11}$$

Crucially, the noncollinear texture is only stable for all values of θ if the spin winding is $l \in \{0, \pm 1\}$. For larger spin windings $|l| \geqslant 2$, we obtain $\mathrm{Im}\,\omega(k) \leqslant 0$ for some $k = 2\pi m/L$ with $m \in \mathbb{Z}$. In Fig. 5(b), we assume $l = 1$. As the phase slip is carried out from $\theta = 0$ (green) to $\theta = \pi$ (orange), the spin-wave dispersion shifts from left to right. While for $\theta = \pi/2$ (orange), the dispersion $\omega(k)$ has a finite and positive imaginary part in the range $-2\pi/L < k < 2\pi/L$ (not shown, but indicated by the flat real part), the imaginary part is always zero at $k = 2\pi m/L$. We remark that the limit $\theta \to 0$ [green curve in Fig. 5(b)] does not coincide with the $j = -j_{\max}$ result in the collinear case [green curve in Fig. 5(a)] because the rotation matrices R in Appendixes H 1 and H 2 differ. In fact, the dispersions agree after shifting the wave number k by p, which stems from the remaining twist of $\mathbf{s}(\ell)$ at $\theta = 0$; see Eq. (H7).

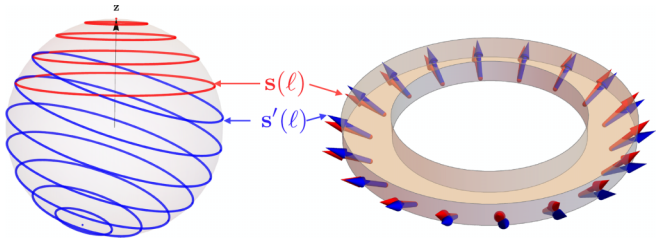

FIG. 6. Mapping of the spin texture $\mathbf{s}(\ell)$ of the ring onto a circle on the sphere, where each point on the sphere represents the direction of $\mathbf{s}$. For the nonsingular phase slip discussed in the main text, the ring sweeps out the sphere symmetrically around the z axis (red circles). However, the system is susceptible to fluctuations of the spin texture from $\mathbf{s}(\ell)$ to $\mathbf{s}'(\ell)$ that can change this symmetry axis (from red to blue circles). This is confirmed in the spin-wave analysis, where we find a zero mode at $k = 2\pi/L$ responsible for these fluctuations.

Including both the dissipation and compressibility again, it is insightful to study the modes with zero frequency, $\omega = 0$. First, we inspect the $k = 0$ modes. We find that the only mode with a nonzero imaginary part is

$$\delta\mathbf{X}(k=0) \propto \begin{pmatrix} \alpha \\ 1 \\ \frac{\alpha pq\sin\theta}{\hbar\chi_w} \\ 0 \end{pmatrix},$$

$$\omega(k=0) = -i\frac{\alpha p^2(1-\kappa)\sin^2\theta}{s\chi_w}. \tag{H12}$$

The imaginary frequency indicates that stability is ensured for $\kappa < 1$. If $\kappa > 1$, this mode corresponds to a runaway nonsingular phase slip that cannot be stabilized at any time. Thus, the noncollinear spin texture becomes unstable for $\kappa > 1$. Nevertheless, the system can still work as a SQUID with abrupt nonsingular phase slips, as discussed in Appendix C.

Another $\omega = 0$ mode exists for $k = 2\pi/L$ if the spin winding is $l = \pm 1$,

$$\delta\mathbf{X}(k = \pm 2\pi/L) \propto \begin{pmatrix} 1 \\ \pm il\cos\theta \\ 0 \\ 0 \end{pmatrix}, \quad \omega(k = \pm 2\pi/L) = 0. \tag{H13}$$

These modes maintain both the skyrmion charge and the exchange energy of the system. They merely change the symmetry axis of the conical spin texture, which for our ansatz is the z axis. By mapping the spin texture $\mathbf{s}(\ell)$ of the ring onto circles on the sphere, where each point indicates its spin orientation (see Fig. 6), these fluctuations rigidly slide the circles around without deformation [from red $\mathbf{s}(\ell)$ to blue $\mathbf{s}'(\ell)$].

[1] D. van Delft and P. Kes, The discovery of superconductivity, Phys. Today **63**, 38 (2010).

[2] J. File and R. G. Mills, Observation of persistent current in a superconducting solenoid, Phys. Rev. Lett. **10**, 93 (1963).

[3] J. P. Sethna, *Statistical Mechanics: Entropy, Order Parameters, and Complexity* (Oxford University Press, Oxford, 2021), Vol. 14.

[4] N. D. Mermin, The topological theory of defects in ordered media, Rev. Mod. Phys. **51**, 591 (1979).

[5] B. I. Halperin, G. Refael, and E. Demler, Resistance in superconductors, Intl. J. Mod. Phys. B **24**, 4039 (2010).

[6] K. Arutyunov, D. Golubev, and A. Zaikin, Superconductivity in one dimension, Phys. Rep. **464**, 1 (2008).

[7] K. Y. Arutyunov, T. T. Hongisto, J. S. Lehtinen, L. I. Leino, and A. L. Vasiliev, Quantum phase slip phenomenon in ultra-narrow superconducting nanorings, Sci. Rep. **2**, 293 (2012).

[8] J. Clarke and A. Braginski, *The SQUID Handbook: Fundamentals and Technology of SQUIDs and SQUID Systems* (Wiley, New York, 2004).

[9] D. Aoki, K. Ishida, and J. Flouquet, Review of U-based ferromagnetic superconductors: Comparison between UGe_2, URhGe, and UCoGe, J. Phys. Soc. Jpn. **88**, 022001 (2019).

[10] X. Liu, Z. Hao, E. Khalaf, J. Y. Lee, Y. Ronen, H. Yoo, D. Haei Najafabadi, K. Watanabe, T. Taniguchi, A. Vishwanath, and P. Kim, Tunable spin-polarized correlated states in twisted double bilayer graphene, Nature (London) **583**, 221 (2020).

[11] A. L. Sharpe, E. J. Fox, A. W. Barnard, J. Finney, K. Watanabe, T. Taniguchi, M. A. Kastner, and D. Goldhaber-Gordon, Emergent ferromagnetism near three-quarters filling in twisted bilayer graphene, Science **365**, 605 (2019).

[12] T. H. Kokkeler, C. Huang, F. S. Bergeret, and I. V. Tokatly, Spectroscopic signature of spin triplet odd-valley superconductivity in two-dimensional materials, Phys. Rev. B **108**, L180504 (2023).

[13] L. Holleis, C. L. Patterson, Y. Zhang, Y. Vituri, H. M. Yoo, H. Zhou, T. Taniguchi, K. Watanabe, E. Berg, S. Nadj-Perge, and A. F. Young, Nematicity and orbital depairing in superconducting Bernal bilayer graphene, Nat. Phys. **21**, 444 (2025).

[14] Y. Zhang, R. Polski, A. Thomson, É. Lantagne-Hurtubise, C. Lewandowski, H. Zhou, K. Watanabe, T. Taniguchi, J. Alicea, and S. Nadj-Perge, Enhanced superconductivity in spin–orbit proximitized bilayer graphene, Nature (London) **613**, 268 (2023).

[15] H. Zhou, L. Holleis, Y. Saito, L. Cohen, W. Huynh, C. L. Patterson, F. Yang, T. Taniguchi, K. Watanabe, and A. F. Young, Isospin magnetism and spin-polarized superconductivity in Bernal bilayer graphene, Science **375**, 774 (2022).

[16] B. Uchoa and A. H. Castro Neto, Superconducting states of pure and doped graphene, Phys. Rev. Lett. **98**, 146801 (2007).

[17] K. Machida and T. Ohmi, Phenomenological theory of ferromagnetic superconductivity, Phys. Rev. Lett. **86**, 850 (2001).

[18] K. V. Samokhin and M. B. Walker, Order parameter symmetry in ferromagnetic superconductors, Phys. Rev. B **66**, 174501 (2002).

[19] A. Huxley, I. Sheikin, E. Ressouche, N. Kernavanois, D. Braithwaite, R. Calemczuk, and J. Flouquet, UGe_2: A ferromagnetic spin-triplet superconductor, Phys. Rev. B **63**, 144519 (2001).

[20] J. Sauls, The order parameter for the superconducting phases of UPt_3, Adv. Phys. **43**, 113 (1994).

[21] M. Sigrist and K. Ueda, Phenomenological theory of unconventional superconductivity, Rev. Mod. Phys. **63**, 239 (1991).

[22] S. Ran, C. Eckberg, Q.-P. Ding, Y. Furukawa, T. Metz, S. R. Saha, I.-L. Liu, M. Zic, H. Kim, J. Paglione, and N. P. Butch, Nearly ferromagnetic spin-triplet superconductivity, Science **365**, 684 (2019).

[23] A. Leggett, The spin dynamics of an anisotropic Fermi superfluid (^{3}He?), Ann. Phys. **85**, 11 (1974).

[24] E. Cornfeld, M. S. Rudner, and E. Berg, Spin-polarized superconductivity: Order parameter topology, current dissipation, and multiple-period Josephson effect, Phys. Rev. Res. **3**, 013051 (2021).

[25] S. K. Kim and S. B. Chung, Current-driven motion of magnetic topological defects in ferromagnetic superconductors, Phys. Rev. B **108**, 134509 (2023).

[26] N. R. Poniatowski, J. B. Curtis, C. G. L. Bøttcher, V. M. Galitski, A. Yacoby, P. Narang, and E. Demler, Surface Cooper-pair spin waves in triplet superconductors, Phys. Rev. Lett. **129**, 237002 (2022).

[27] E. I. Blount and C. M. Varma, Electromagnetic effects near the superconductor-to-ferromagnet transition, Phys. Rev. Lett. **42**, 1079 (1979).

[28] A. Brataas and Y. Tserkovnyak, Spin and charge pumping by ferromagnetic-superconductor order parameters, Phys. Rev. Lett. **93**, 087201 (2004).

[29] N. D. Mermin and T.-L. Ho, Circulation and angular momentum in the a phase of superfluid helium-3, Phys. Rev. Lett. **36**, 594 (1976).

[30] T.-L. Ho, Coreless vortices in superfluid ^{3}He-a: Topological structure, nucleation, and the screening effect, Phys. Rev. B **18**, 1144 (1978).

[31] M. Tinkham, *Introduction to Superconductivity*, 2nd ed. (NY: Dover Publications, Mineola, 2004).

[32] More generally, the complex order parameter is $\mathbf{d}(\mathbf{r}) = d(\mathbf{r})e^{i\phi(\mathbf{r})}[\mathbf{e}_1(\mathbf{r}) + i\mathbf{e}_2(\mathbf{r})]/\sqrt{2}$, which yields the winding $w_i = \partial_i\phi + \mathbf{e}_1 \cdot \partial_i\mathbf{e}_2$. Here, we have made the gauge choice $\phi = 0$, which results in $\mathbf{w}$ being identified with the connection. For a full gauge-independent formulation, see Appendix A.

[33] C. Dao, J. Zou, E. Kleinherbers, and Y. Tserkovnyak, Topological transport of vorticity on curved magnetic membranes, Phys. Rev. B **111**, L100401 (2025).

[34] R. D. Kamien, The geometry of soft materials: A primer, Rev. Mod. Phys. **74**, 953 (2002).

[35] J. Zou, S. K. Kim, and Y. Tserkovnyak, Topological transport of vorticity in Heisenberg magnets, Phys. Rev. B **99**, 180402(R) (2019).

[36] W. Koshibae and N. Nagaosa, Creation of skyrmions and antiskyrmions by local heating, Nat. Commun. **5**, 5148 (2014).

[37] A. Hatcher, *Algebraic Topology* (Cambridge University Press, Cambridge, 2002).

[38] T. Machon and G. P. Alexander, Global defect topology in nematic liquid crystals, Proc. R. Soc. A **472**, 20160265 (2016).

[39] F. N. Rybakov, O. Eriksson, and N. S. Kiselev, Topological invariants of vortices, merons, skyrmions, and their combinations in continuous and discrete systems, Phys. Rev. B **111**, 134417 (2025).

[40] P. W. Anderson and G. Toulouse, Phase slippage without vortex cores: Vortex textures in superfluid ^{3}He, Phys. Rev. Lett. **38**, 508 (1977).

[41] A. Knigavko, B. Rosenstein, and Y. F. Chen, Magnetic skyrmions and their lattices in triplet superconductors, Phys. Rev. B **60**, 550 (1999).

[42] M. Nakahara, *Geometry, Topology and Physics* (CRC Press, Boca Raton, FL, 2018).

[43] If $\mathcal{C}$ can be identified with the boundary $\partial\mathcal{A}$ of a simply connected superconducting patch $\mathcal{A}$ without any singularities, then the texture on $\mathcal{C}$ is restricted to the even sector.

[44] Note that for $q = -2e < 0$, the magnetic flux quantum Φ_0 as well as j_0 are negative.

[45] P. A. M. Dirac, Quantised singularities in the electromagnetic field, Proc. R. Soc. A **133**, 60 (1931).

[46] Q. Peng, S. McMurry, and J. Coey, Axial magnetic field produced by axially and radially magnetized permanent rings, J. Magn. Magn. Mater. **268**, 165 (2004).

[47] W. A. Little and R. D. Parks, Observation of quantum periodicity in the transition temperature of a superconducting cylinder, Phys. Rev. Lett. **9**, 9 (1962).

[48] L. D. Jackel and R. A. Buhrman, Noise in the RF SQUID, J. Low Temp. Phys. **19**, 201 (1975).

[49] E. Sonin, Spin currents and spin superfluidity, Adv. Phys. **59**, 181 (2010).

[50] Y. Zhu, E. Kleinherbers, L. Levitov, and Y. Tserkovnyak, Proposal for spin superfluid quantum interference device, Phys. Rev. B **112**, L100405 (2025).

[51] P. M. Chaikin and T. C. Lubensky, *Principles of Condensed Matter Physics* (Cambridge University Press, Cambridge, 1995).

[52] B. U. Felderhof, V. V. Sokolov, and P. A. Éminov, Hamiltonian field theory of ferrohydrodynamics, J. Chem. Phys. **135**, 144901 (2011).

[53] P. J. Morrison, Hamiltonian description of the ideal fluid, Rev. Mod. Phys. **70**, 467 (1998).

[54] G. E. Volovik, *The Universe in a Helium Droplet* (Oxford University Press, Oxford, 2009).

[55] L. Onsager, Reciprocal relations in irreversible processes. I, Phys. Rev. **37**, 405 (1931).

[56] L. D. Landau and E. M. Lifshitz, *Statistical Physics, Part 1*, Course of Theoretical Physics Vol. 5 (Butterworth-Heinemann, Oxford, 1980).

[57] D. Vollhardt and P. Wolfle, *The Superfluid Phases of Helium 3* (Taylor and Francis, Philadelphia, PA, 1990).

[58] R. Blaauwgeers, V. B. Eltsov, M. Krusius, J. J. Ruohio, R. Schanen, and G. E. Volovik, Double-quantum vortex in superfluid ^{3}He-A, Nature (London) **404**, 471 (2000).

[59] G. E. Volovik, Vortices observed and to be observed, J. Low Temp. Phys. **121**, 357 (2000).

[60] R. E. Packard and Y. Sato, Superfluid helium quantum interference devices (SHeQUIDs): Principles and performance, J. Phys.: Conf. Ser. **568**, 012015 (2014).

[61] V. V. Dmitriev, M. S. Kutuzov, A. A. Soldatov, and A. N. Yudin, Superfluid β phase of ^{3}He, Phys. Rev. Lett. **127**, 265301 (2021).

[62] J. Liu, V. Subramanyan, R. Welser, T. McSorley, T. Ho, D. Graf, M. T. Pettes, A. Saxena, L. E. Winter, S.-Z. Lin, and L. A. Jauregui, Possible spin-triplet excitonic insulator in the ultra-quantum limit of $HfTe_5$, Phys. Rev. Lett. **135**, 046601 (2025).

[63] H. Bulou, L. Joly, J.-M. Mariot, and F. Scheurer, *Magnetism and Accelerator-based Light Sources* (Springer Nature, New York, 2021).

[64] A. J. Leggett, A theoretical description of the new phases of liquid ^{3}He, Rev. Mod. Phys. **47**, 331 (1975).

[65] S. R. De Groot and P. Mazur, *Non-Equilibrium Thermodynamics* (NY: Dover Publications / Courier Corporation, Mineola, 2013).

[66] J. R. Schaibley, H. Yu, G. Clark, P. Rivera, J. S. Ross, K. L. Seyler, W. Yao, and X. Xu, Valleytronics in 2D materials, Nat. Rev. Mater. **1**, 16055 (2016).

[67] E. Kleinherbers, T. Stegmann, and N. Szpak, Electronic transport in bent carbon nanotubes, Phys. Rev. B **107**, 195424 (2023).

[68] P. Coleman, *Introduction to Many-body Physics* (Cambridge University Press, Cambridge, 2015).

[69] We remark that the amplitude $f_{\mathbf{k}} = v_{\mathbf{k}}/u_{\mathbf{k}}$ by using the Bogoliubov coherence factors.

[70] M. Combescot and S.-Y. Shiau, *Excitons and Cooper Pairs: Two Composite Bosons in Many-body Physics* (Oxford University Press, Oxford, 2015).

[71] J. da Providencia and C. Fiolhais, Variational principles in quantum statistical mechanics, Eur. J. Phys. **8**, 12 (1987).

[72] A. Brataas, Y. Tserkovnyak, G. E. W. Bauer, and P. J. Kelly, Spin pumping and spin transfer, in *Spin Current*, edited by S. Maekawa, S. O. Valenzuela, E. Saitoh, and T. Kimura (Oxford University Press, Oxford, 2017).

[73] G. E. Volovik, Poisson bracket scheme for vortex dynamics in superfluids and superconductors and the effect of the band structure of the crystal, JETP Lett. **64**, 845 (1996).

[74] D. D. Holm and B. A. Kupershmidt, Poisson structures of superconductors, Phys. Lett. A **93**, 177 (1983).

[75] A. S. Bradley, R. K. Kumar, S. Pal, and X. Yu, Spectral analysis for compressible quantum fluids, Phys. Rev. A **106**, 043322 (2022).

[76] A. A. Belavin and A. M. Polyakov, Metastable states of two-dimensional isotropic ferromagnets, JETP Lett. **22**, 245 (1975).

[77] H. K. Moffatt, The degree of knottedness of tangled vortex lines, J. Fluid Mech. **35**, 117 (1969).

[78] H. Helmholtz, LXIII. On integrals of the hydrodynamical equations, which express vortex-motion, London, Edinburgh, Dublin Philos. Mag. J. Sci. **33**, 485 (1867).

[79] V. Kozlov and A. Samokhvalov, Closed Abrikosov vortices in a superconducting cylinder, Physica C **213**, 103 (1993).

[80] L. Woltjer, A theorem on force-free magnetic fields, Proc. Natl. Acad. Sci. USA **44**, 489 (1958).

[81] M. A. Berger, Introduction to magnetic helicity, Plasma Phys. Control. Fusion **41**, B167 (1999).

[82] R. Shankar, Applications of topology to the study of ordered systems, J. Phys. France **38**, 1405 (1977).

[83] T. H. R. Skyrme, A non-linear field theory, Proc. R. Soc. Lond. Ser. A **260**, 127 (1961).

[84] Y. Liu, H. Watanabe, and N. Nagaosa, Emergent magnetomultipoles and nonlinear responses of a magnetic hopfion, Phys. Rev. Lett. **129**, 267201 (2022).

[85] P. Sutcliffe, Hopfions in chiral magnets, J. Phys. A: Math. Theor. **51**, 375401 (2018).

[86] J. Zou, S. Zhang, and Y. Tserkovnyak, Topological transport of deconfined hedgehogs in magnets, Phys. Rev. Lett. **125**, 267201 (2020).